NTNU

Norwegian University of
Science and Technology

Developing an Application for Simulating a Parametrized PM Machine by FEM

Hallvar Haugdal

Master of Energy and Environmental Engineering
Submission date: March 2016
Supervisor: Robert Nilssen, ELKRAFT

Norwegian University of Science and Technology
Department of Electric Power Engineering

Developing an Application for Simulating a Parametrized PM Machine by FEM

Hallvar Haugdal

Department of Electrical Power Engineering
Norwegian University of Science and Technology (NTNU)
Trondheim
Email: hallvhau@stud.ntnu.no

***Abstract*—A parametrized 2D model of a permanent magnet synchronous machine is developed in the finite elements method software COMSOL Multiphysics, along with a graphical user interface to control it. The GUI provides automatic construction of geometry based on specified input parameters, application of boundary conditions and equations, and post-processing of results. Algorithms are implemented to apply automatic periodicity settings and winding layouts for single layer and double layer integer and fractional slot windings. The output of the model is validated by comparing to analytical formulas and to other studies with known input parameters and results.**

The purpose of developing the the application is educational, allowing simulations to be performed without requiring in-depth knowledge of FEM. A range of sample studies are presented in this respect, to indicate possible areas of application within the educational setting. It is found that simulations can be performed very efficiently, indicating that the application could provide a valuable tool for studying electrical machines. Depending on further development and implementation of additional functionality, the application could probably also be used in the process of designing machines.

March 7, 2016

NOMENCLATURE

p	number of rotor poles
Q	number of stator slots
q	number of slots per pole and phase
l	axial length
$R_{s,out}$	outer stator radius
$R_{s,in}$	inner stator radius
$R_{r,out}$	outer rotor radius
$R_{r,in}$	inner rotor radius
S_d	stator slot depth
S_w	stator slot width, relative
R_{PM}	PM radius
PM_h	PM height
PM_w	PM width, relative
PM_{br}	PM flux remanence
N_{rep}	periodicity of machine
N_t	total number of series connected turns
$N_{t,coil}$	number of turns per coil
N_{par}	number of parallel connections
l_g	length of air gap
t	time
u	parametric sweep variable
ω	electrical frequency [rad/s]
T	electrical period
I	current amplitude
V	voltage amplitude
E	internal generated voltage
P	power
τ	torque
W	magnetic energy
β	angle with which current lags d-axis
k_w	winding factor
θ_{wind}	spatial angle of winding
X_d	direct axis reactance
X_q	quadrature axis reactance
L	synchronous inducance
M	mutual inducance
L_l	leakage inductance
L_s	self inductance (single phase)
$L_{m,1ph}$	single phase magnetizing inductance
$L_{m,3ph}$	three phase magnetizing inductance

I. INTRODUCTION

The first papers describing solution of electrical engineering problems by FEM were published in 1968 [18]. Since then the method has become the first choice for solving problems involving partial differential equations where analytical solutions are hard and tedious to derive. When applied to electrical machine analysis, the geometry is often highly similar within the machine topologies, resulting in very similar FEM problem formulations to be solved. This makes the case for implementing a parametrized model of a machine, where construction of geometry and application of boundary conditions and field equations are carried out automatically.

In recent years programs such as `COMSOL Multiphysics` and `ANSYS` have become increasingly available, allowing engineers and students to deploy FEM without requiring in-depth knowledge of the underlying mathematics. A recent addition in `COMSOL` takes this a step further; the newly embedded *Application Builder* allows a GUI to be implemented to control the model, thus requiring the user of the application to know merely what phenomenon is being studied, and what to make of the results.

The two above arguments, in combination with the power of desktop computers reaching a level where advanced FEM calculations can be performed within minutes, motivates the implementation of a parametrized model of an electrical machine along with a GUI to control it.

To keep the scope within range for this thesis, the range of machines available by varying parameters of the model are all PM Synchronous Machines with internal rotor, where the PMs are radially magnetized and the stator is slotted with a Double Layer or Single Layer Lap Winding. The model is current fed, i.e. load conditions are specified as magnitude and angle of the current. Losses are neglected. The permeability of iron is assumed constant, not taking saturation into account. No particular distinction is made between generator and motor, letting this result solely as a consequence of the angle between the stator and rotor fields. The rotor rotation is specified as a function of time only, not taking mechanics into account.

The model is simulated stationarily and in time, with functionality allowing parametric sweeps to be performed, in which a series of simulations are conducted while changing a geometric parameter (radius, PM width, etc.) or operation condition (load current, frequency, etc) between each simulation.

The main purpose of the Application at this point is educational. However, the parametrized model could also be used in a consultant application, for instance in performing an optimization procedure related to some particular machine application.

The development of the Application, comprised of a FEM Model and a GUI, is described in six main sections:

Theory The theoretical basis from which the model is built is presented. Maxwell's Equations and FEM are reviewed briefly, as well as some theory specific to electrical machines, regarding among others winding layout, periodicity and torque calculations.

The Model The development of the model in `COMSOL` is described, considering geometric construction, application of physical relations, meshing and post-processing.

The Application The layout and functioning of the Application are described, as well as the implementation of some of the more advanced routines.

Validation of The Model The output of the model is compared to analytical formulas to indicate whether or not the model produces valid results. In addition, two studies with known input parameters and results are recreated, attempting to arrive at the same results with this model.

Example Studies A number of example studies are presented, which are quite straight forward to set up with the Application, indicating some ways in which the Application is thought to be used.

Discussion The Application is evaluated regarding among others viability, areas of application and possible improvements.

II. Theory

A. Maxwell's Equations

To determine the performance of a machine without building it in real life, a lot if information is revealed by solving Maxwell's Equations on a geometry resembling the machine. The four equations, reproduced below, describe the electromagnetic phenomena acting in a machine very accurately, allowing characteristics like inductances, torque production and induced voltage to be estimated.

$$\nabla \cdot \mathbf{D} = \rho \tag{1a}$$

$$\nabla \cdot \mathbf{B} = 0 \tag{1b}$$

$$\nabla \times \mathbf{E} = -\frac{\partial \mathbf{B}}{\partial t} \tag{1c}$$

$$\nabla \times \mathbf{H} = \frac{\partial \mathbf{D}}{\partial t} + \mathbf{J} \tag{1d}$$

When solving Maxwell's equations, it is often convenient to express the fields in terms of potentials, and then deriving the fields from these. The Magnetic Vector Potential [18] is given by

$$\mathbf{E} = -\nabla\phi - \frac{\partial \mathbf{A}}{\partial t} \tag{2a}$$

$$\mathbf{B} = \nabla \times \mathbf{A}. \tag{2b}$$

By inserting the expressions into Equation 1b and Equation 1c it is found that these two equations are automatically satisfied.

The vector potential is not uniquely defined from the above relation, as a divergence component can be introduced without altering the potential. Specifying the divergence is often referred to as gauge fixing, and the two most frequently used choices are the *Lorentz gauge* and the *Coulomb Gauge*. In a two-dimensional approximation, it can be shown [14] that the latter is automatically satisfied.

B. FEM

Analytical solutions of the field equations are generally hard to derive, except for on trivial geometries. Gysen et al. [6] also proposes a comprehensive method utilizing Fourier Analysis to calculate the fields, which is applicable on more general electrical machine geometries. For the parametrized model developed here, FEM is considered a suitable way of calculating the fields, due to the ability of providing a solution for an arbitrary geometry, given that the proper boundary conditions and field equations are applied.

The theory behind FEM is not described in detail here. Rather, some basic principles of the method are outlined.

By using FEM a problem consisting of few, complicated equations that are difficult to solve, is transformed into many simple equations that can be solved by general methods for systems of equations.

The sub domains of the geometry on which the field equations are solved are divided into elements, often triangular or quadrilateral in two dimensional problems. The corners of

the elements are connected to neighboring elements in nodes, such that the elements constitute a mesh.

The approximation of the final solution within an element is given as an interpolation of the values of the solutions on the corner nodes of the element. The problem then becomes that of finding the solution in the corner nodes. This can be approached in many ways, generally resulting in a linear system of equations to be solved, which can be stated on the form

$$\mathbf{AU} = \mathbf{b}, \tag{3}$$

where $\mathbf{U}$ is a vector containing the solutions in the nodes and $\mathbf{b}$ is determined by boundary conditions. The matrix $\mathbf{A}$ is often found to be sparse and diagonally dominant, i.e. containing elements mainly along its diagonal, which is advantageous when solving the system.

COMSOL performs the underlying mathematics of FEM automatically, allowing the user to focus solely on specifying the geometry and physics, and reviewing results. This process is not trivial either, requiring thorough knowledge of the functioning of the object being modeled, in this case an electrical machine, to arrive at a well posed problem formulation, and to determine whether the results make sense or not.

C. PM Machines

Electrical motors generally function by producing torque as two sources of magnetic fields try to align within the machine. One field is set up by a source mounted on a rotating member, the rotor, and the other on a stationary member, the stator. By rotating one of the fields with respect to the member on which its source is situated, forces act to keep the fields aligned, resulting in a mechanical torque at the shaft of the rotor.

Rotation of magnetic fields can be achieved with a series of coils placed at different angular positions, and then exciting the coils successively. This is essentially what happens in a three phase AC winding.

Electrical generators are in principle the same machines as motors. In a machine operating as a generator, a torque applied at the rotor causes relative motion between conductors and a magnetic field. A voltage is induced in the conductors, allowing mechanical energy to be converted to electrical energy.

In PM synchronous machines the rotor field is set up by PMs, while the stator field is set up by multi phase AC currents around the stator. For a motor to produce a high torque relative to its size, and a generator to generate a high voltage, the coils around the stator are arranged such as to maximize these. The coils are often positioned in slots in the stator, such that the freedom in specifying their position is constrained by the position of the slots. All the coils of the stator constitute the Winding, and the specific arrangement of the coils is referred to as the Winding Layout, which depends mainly on the number of magnetic poles (p) in the rotor field and the number of slots (Q) in the stator.

D. Windings in Electrical Machines

The winding layouts performed here are Single Layer or Double Layer Windings consisting of a number of equal Lap Wound coils. The layout is performed by utilizing a Slot Star, discussed below, providing layouts for both Integer- and Fractional Slot Windings, characterized by the number of slots per pole per phase,

$$q = \frac{Q}{mp} = I + \frac{n}{d}, \tag{4}$$

being an integer or a fraction, respectively. Q is the number of slots, m is the number of phases and p is the number of poles. n and d are integers with no common divisor.

Machines with the same value of q generally have a highly similar winding layout, but possibly differing in the number of repetitions of the same base winding [14]. For machines with double layer windings the number of repetitions, often referred to as the periodicity of the machine [3], is given by

$$N_{rep} = \gcd(p, Q). \tag{5}$$

A similar expression is presented later, describing the periodicity in machines with single layer windings.

For integer slot machines ($q = I$ in Equation 4), the periodicity is simply p, such that the base winding comprises $3 \cdot I$ slots spanning one pole, repeated p times around the stator. Fractional slot machines are also often periodic, but with a lower number of repetitions.

For the layout to be three phase symmetric, two constraints are imposed on the combination of the number of slots Q and poles p [14]. The first constraint is, for a double layer winding and single layer winding respectively,

$$\frac{Q}{3} \in \mathbf{N} \qquad\qquad \frac{Q}{6} \in \mathbf{N}, \tag{6}$$

where $\mathbf{N}$ is the set of all natural numbers, i.e. not fractions. This first condition simply states that there must be an equal number of slots assigned to each phase, and ensuring space for a return conductor for each coil for the single layer winding. The second condition is

$$\frac{d}{3} \notin \mathbf{N}, \tag{7}$$

where d refers to the denominator in Equation 4.

1) Slot Star: The winding layout is carried out, according to Sequenz [17], by drawing a phasor diagram describing the electrical angle of each slot in the rotor field, and assigning phasors contributing in the same direction to the same phase.

The electrical angle between adjacent stator slots is given by

$$\epsilon = \frac{p}{2Q} 2\pi. \tag{8}$$

Drawing a phasor diagram where slot i is represented by a phasor of magnitude 1 and angle $\epsilon \cdot i$, it becomes evident which phasors should be assigned to the respective phases. The circumferential span of 360 °is divided into 6 equal sectors

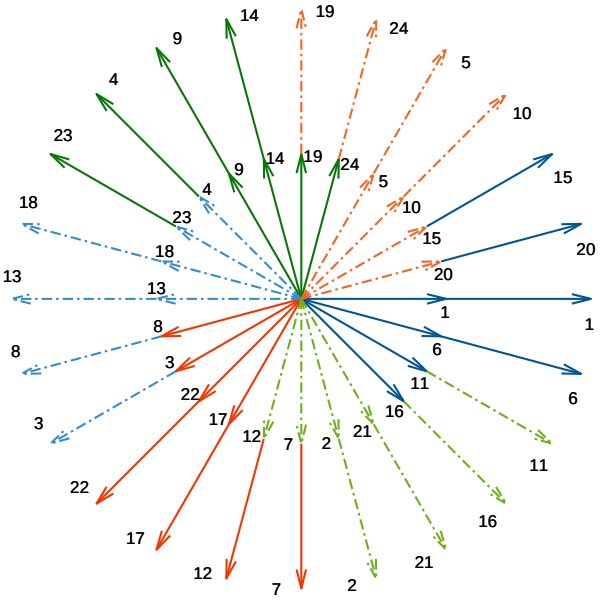

Figure 1: Slot Star describing a Double Layer Winding in a 10p, 24S-machine.

of 60 °, where each sector represents the phase-polarity group (A+, A-, B+....) to which the phasors within the sector are to be assigned.

2) Double Layer Winding: Considering a double layer winding, each slot contains two conductors, resulting in twice as many phasors in the slot star. When assigning phasors to phase-polarity groups, only one of the layers is considered, thus letting the second layer result as a direct consequence of the first layer and the coil span. The coil span (expressed as an integer number of slots) is given the value

$$c_{span} = \texttt{round}\left(\frac{Q}{p}\right), \tag{9}$$

which places the return conductor in the slot where the electrical angle difference from the slot of the first conductor is closest to 180°(and less than 360°). Thus, phasor i represents the coil whose first conductor lies in slot i, and return conductor lies in slot $i + c_{span}$. The resulting layout from this method is shown for a 10p 24S-winding in Figure 1.

3) Single Layer Winding: The single layer winding layout is based on a method proposed by Bianchi and Prè [3], where a conventional double layer winding is converted into a single layer winding by removing every other coil around the stator. For the single layer winding to be feasible, the number of slots must be divisible by two, ensuring space for return conductors in every other slot. Also, the coil span in the initial double layer layout should be odd, such that the return conductors fill the empty spaces between the other conductors. However, to be able to perform a Single Layer layout for as many poles/slots-combinations as possible, though possibly deteriorating the winding factor, the coil span is assigned the value

$$c_{span} = 1 + 2 \cdot \texttt{round}\left(\frac{\frac{Q}{p} - 1}{2}\right), \tag{10}$$

which is similar to Equation 9, but ensures that the coil span is odd.

Other single layer winding layout methods exist [14] that result in higher winding factors, but depend on being able to change the coil span around the stator. However, the simple method presented still provides many useful layouts, especially some commonly used configurations with a low value of q, for instance 10p 12S and 22p 24S.

The conversion from a double layer winding to a single layer winding alters the periodicity of the machine. Intuitively, since a single layer winding consists of half the number of coils compared to a double layer winding, it can be thought of as a double layer winding layout performed for half the number of slots $\left(\frac{Q}{2}\right)$. Then, inserting this double layer winding into every other slot of the machine with Q slots and altering the coil span such that the return conductors fill the empty slots, a single layer layout is achieved. This way of thinking of the single layer winding is also justified by the fact that when assigning slots to phases using the slot star, the decision is made solely based on the relative position of the slots compared to the rotor field; thus, slots $1, 2, 3$ in a winding with $\frac{Q}{2}$ slots are assigned to the same phases as slots $1, 3, 5$ in a winding with Q slots.

The periodicity of the single layer winding then becomes that of the double layer winding with half the number of slots,

$$N_{rep} = \texttt{gcd}\left(p, \frac{Q}{2}\right). \tag{11}$$

However, it turns out that the periodicity can be increased in some cases. By observing that in double layer integer slot windings with full coil pitch, the two conductors in each slot always belong to the same phase. It turns out that this is reproducible by a single layer winding (except resulting in half the number of possible parallels); therefore, it is found that also the periodicity must be similar, i.e. as given by Equation 5 for single layer integer slot windings.

4) Winding Factor and Spatial Angle: By vector summation of the phasors in the slot star belonging to the same phase, the winding factor is calculated as

$$k_w = \frac{|\sum \mathbf{v}|}{Q_{ph}}, \tag{12}$$

where Q_{ph} is the number of coils in each phase. Also, the angle of the vector,

$$\theta_{wind} = \angle \sum \mathbf{v} \tag{13}$$

determines the relation between space vectors and phase quantities: If this angle is subtracted from the angle of the current, the stator field at $t = 0$ will be directed $90° \cdot \frac{2}{p}$ clockwise of the horizontal axis in space (if current in the positive z-axis direction is out of the plane). This can then be

utilized to relate the stator field to the d- and q-axis, which are known from the orientation of the rotor.

E. Periodicity

As mentioned, electrical machines often posess a high degree of symmetry. This can be taken advantage of in simulation, as the performance of a machine can be assessed by considering only a fraction of it. The degrees of freedom of the problem are reduced correspondingly, resulting in a less computationally demanding problem.

The number of symmetric sectors in a machine is similar to the number of repetitions of the base winding, as mentioned in subsection II-D, i.e. given by Equation 5 for all Double Layer Windings and Single Layer Integer Slot Windings, and Equation 11 for Single Layer Fractional Slot Windings. To utilize this in simulation, only one instance of the sector containing the base winding is drawn. Then specific periodic boundary conditions are applied to the resulting sector boundaries in the circumferential direction, and on the boundary between the stationary and rotating regions.

Taking advantage of periodicity in simulation results in fewer degrees of freedom of the problem to be solved. However, the problem generally takes longer to solve than a non-periodic problem with the same number of degrees of freedom. This is due to the matrix A in Equation 3 being less diagonally dominant, i.e. containing more elements far away from the diagonal. Ultimately this results in slower convergence when solving the system of equations.

F. Torque Calculations

Accurate torque calculations require high element densities, and thus excessive computing power. The standard method in COMSOL is based on integration of Maxwell's Stress Tensor over a cylinder surface enclosing the rotor. Another method, considered less prone to numerical error [14], is proposed by Arkkio [1], where the following expression is integrated over a thin cylinder volume in the air gap,

$$\tau = \frac{l}{\mu_0(r_o - r_i)} \int_S r B_r B_\phi \mathrm{d}S, \tag{14}$$

where r_o and r_i denotes the respective inner and outer radiuses of the cylinder, and l the axial length of the machine. r is the radius at which the expression is being evaluated, and B_r and B_ϕ are the radial- and circumferential components of the **B**-field. The method is commonly referred to as Arkkios Method.

When assessing no load cogging torque in a machine, it is convenient to simulate only one period of the cogging torque cycle. The mechanical rotation per cycle is related to the number of poles and slots [8] by the equation

$$\alpha_{cog} = \frac{2\pi}{\mathtt{lcm}(Q,p)}, \tag{15}$$

where lcm denotes the Least Common Multiple. Relating this to electrical frequency, the period of one cogging torque cycle is found to be

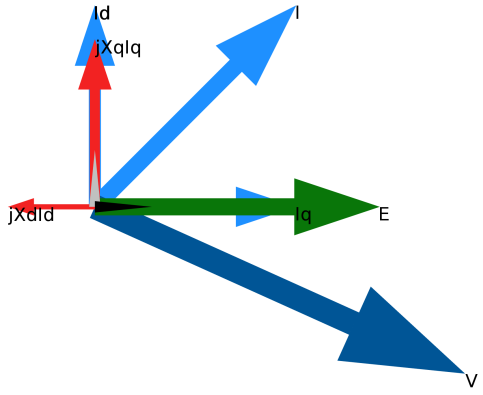

Figure 2: Phasor diagram corresponding to Synchronous Machine Equivalent Circuit. The diagram shows a machine operating as a generator ($I_q > 0$) consuming reactive power ($I_d > 0$). The q-axis reactance is larger than the d-axis reactance.

$$T_{cog} = \frac{1}{\omega} \cdot \frac{p}{2} \cdot \alpha_{cog} = \frac{T \cdot p}{2 \cdot \mathtt{lcm}(Q,p)}, \tag{16}$$

where T and ω refer to electrical period and frequency (rad/s).

The amplitude of the torque ripple in a machine generally decreases as the value of $\mathtt{lcm}(Q,p)$ increases [9], requiring an increasingly dense mesh to achieve good results. Relating this to machine periodicity, and noting that

$$\mathtt{lcm}(Q,p) = \frac{Qp}{\mathtt{gcd}(Q,p)},$$

it is found that low periodicity is associated with low cogging torque, explaining why accurate cogging torque assessment in fractional slot machines is generally associated with excessive computations. Alternative methods for calculating torque ripple have been proposed to limit the demand on computing power, for instance as described by Hsiao et al.; utilizing the "half magnet pole pair"-method, a highly accurate FEM calculation is performed to evaluate the interaction between only a small part of the rotor and the complete stator, and then superposing the contributions from all the rotor poles to achieve the resulting torque ripple in the machine. This is performed for a machine with 96p and 100S. Computations of this magnitude are outside the intended scope of the model developed here.

G. Equivalent Circuit

The synchronous machine operating in steady state can be modeled by a simple electrical circuit [4]; the internal generated voltage (E) is modeled as a sinusoidal voltage source, the armature reaction is modeled as a voltage drop across the synchronous reactance (X), and the sum of the two contributions results in the terminal voltage (V). Also,

to account for saliency, the current can be decomposed into its direct (d) and quadrature (q) axis components, allowing saliency to be modeled by the respective direct and quadrature axis reactances (X_d) and (X_q). As the model implemented here does not take losses into account, a resistance term is not included. The resulting circuit equation is

$$E = V + jX_dI_d + jX_qI_q, \tag{17}$$

with the corresponding phasor diagram shown in Figure 2.

When considering generator operation, it is customary to define the direction of the current as above, i.e. positive when the machine is delivering electrical power. However, the equivalent circuit is valid also for motor operation, only differing from the usual synchronous motor circuit in that the direction of the current is opposite.

The d-axis is aligned with the magnetic field from the rotor PMs, and the q-axis is orthogonal to it. The choice of whether to define the q-axis as leading [12] or lagging [11] the d-axis might also be taken based on whether a generator or a motor is being studied: In a generator producing electrical power, the stator field lags the rotor field; therefore, for a positive q-axis current to be associated with power production, the q-axis should be defined as lagging the d-axis.

From the angle of the rotor, the d- and q-axis angles are always known, and since the model is current fed, the angle and magnitude of the current vector are also known. In addition, if a study was conducted in time, the magnitude and angle of the voltage phasor can be found from the coefficients of the fundamental in the Fourier Series, presented later in subsection II-I. The internal generated voltage (E) can be found by performing a no-load simulation, where there is no current and the internal generated voltage equals the terminal voltage.

Equation 17 can then be solved for d- and q-axis reactances. Summing contributions in the directions of the d- and q-axis separately, and noting that E is directed along the q-axis, gives

$$X_d = \frac{V_q - E}{I_d} \tag{18}$$

$$X_q = -\frac{V_d}{I_q}, \tag{19}$$

where V_d and V_q are projections of V along the d- and q-axes.

H. Current Excitation

The model developed is current fed, i.e. the excitation of the stator winding is specified as angle and amplitude of current. This choice is made solely due to a more straight forward implementation than with a voltage excited model.

A Torque Angle Characteristic [11] of a machine is customarily rendered as the torque at different load angles, i.e. the angle between terminal voltage (V) and internal generated voltage (E), while holding the voltage magnitudes constant. This model being current fed, a similar characteristic is instead obtained by holding the current constant and varying the current angle around the no load point. If the angle is such that it produces a flux directed along the d-axis, no torque is developed. If the current leads or lags the d-axis, the machine operates respectively as a motor or generator. The angle between the current and the d-axis is defined as β; associating a positive angle with positive q-axis current (generator operation) gives tthe d-and q-axis decompositions $I_d = I\cos\beta$ and $I_q = I\sin\beta$. This allows the following characteristic to be derived:

$$\begin{aligned}\frac{1}{3}\tau\omega &= \frac{1}{3}P \\ &= V_dI_d + V_qI_q \\ &= (-X_qI_q)I_d + (E + X_dI_d)I_q \\ &= (X_d - X_q)I_dI_q + EI_q \\ &= (X_d - X_q)I^2\cos\beta\sin\beta + EI\sin\beta \\ &= (X_d - X_q)\frac{I^2}{2}\sin 2\beta + EI\sin\beta,\end{aligned} \tag{20}$$

which can be solved for torque. The first term of the expression corresponds to the Reluctance Torque, which gives a positive contribution around the no-load angle ($\beta = 0$) for salient pole machines. In machines with cylindrical rotors, the torque is given only by the second term, which is referred to as the Cylindrical Torque.

I. Induced Voltage

The induced voltage can be calculated from the electrical field [13] by integrating the z-component of the field over an area corresponding to the cross section of a conductor A_c, and multiplying by the axial length of the machine l:

$$V = \frac{l}{A_c} \cdot \int_S E_z \,\mathrm{d}S. \tag{21}$$

This is the voltage resulting from the contributions of the internal generated voltage and the armature reaction, discussed in subsection II-G. In the lossless case this is equal to the phase to ground voltage.

This voltage generally contains of harmonics from the rotor field. The amplitudes of these can be calculated as the coefficients of the Fourier Series, given by

$$a_n = \frac{2}{T}\int_0^T v(t)\cos(n\omega t)\,\mathrm{d}t \tag{22}$$

$$b_n = \frac{2}{T}\int_0^T v(t)\sin(n\omega t)\,\mathrm{d}t, \tag{23}$$

with the magnitude and angle given by

$$V_n = \sqrt{a_n^2 + b_n^2}, \tag{24}$$

$$\delta_n = \arctan\left(\frac{b_n}{a_n}\right). \tag{25}$$

Setting n=1 gives the magnitude and angle of the fundamental frequency.

1) Analytical Expression: If the flux set up by the PMs along the air gap is assumed to be a square wave, which is roughly the case if the PMs are surface mounted, radially magnetized and the width of the magnets is such that they fill the complete circumference ($PM_w = 2\pi R_{PM}/p$), the voltage induced in a full pitch stator coil with N_t turns by a rotating PM can be found by

$$\begin{aligned} e_{coil} &= 2N_t e_{cond} = 2N_t(B_{AG}vl) \\ &= 2N_t \frac{\Phi_{AG}}{\left(\frac{2\pi R_{AG}}{p}\right)}(R_{AG}\omega_m)l \\ &= \frac{N_t \omega_m l p}{\pi}\Phi_{AG}. \end{aligned} \tag{26}$$

where v is the speed of the PMs. The field set up by the PMs can be found from a magnetic circuit consisting of a current source connected to two resistances in parallel. The current source represents the remanent flux in the PMs (Φ_r), and the resistances represent the PM reluctance ($\mathcal{R}_{PM}$) and air gap reluctance ($\mathcal{R}_{AG}$), respectively. Assuming relative permeability of PMs equal to air, this gives the flux through the air gap

$$\begin{aligned} \Phi_{AG} &= \Phi_r \frac{\mathcal{R}_{PM}}{\mathcal{R}_{PM} + \mathcal{R}_{AG}} \\ &= \Phi_r \frac{l_{PM}}{l_{PM} + l_{AG}}. \end{aligned} \tag{27}$$

Expressing the remanent flux in terms of remanent flux density B_r gives

$$\begin{aligned} \Phi_r &= B_r A_{PM} \\ &= B_r \cdot \frac{2\pi R_{PM}}{p} \end{aligned} \tag{28}$$

Inserting Equation 27 and Equation 28 into Equation 26 gives

$$e = 2N_t \omega_m l \cdot B_r R_{PM} \frac{l_{PM}}{l_{PM} + l_{AG}}. \tag{29}$$

J. Inductance Calculations

The inductances in a machine can be obtained in a number ways, besides from the phasor diagram as outlined in subsection II-G. If only one phase, say A, is excited with a sinusoidal voltage or current, the Self Inductance can be found from the resulting amplitudes of the voltage and current,

$$\omega L_s = \frac{V_a}{I_a}. \tag{30}$$

Similarly, by measuring the induced voltage in one of the other phases, say B, under the same conditions, the Mutual Inductance between phases can be found by

$$\omega M = \frac{V_b}{I_a}. \tag{31}$$

The Self Inductance can be decomposed into two parts: The flux crossing the air gap can be attributed to the Single Phase Magnetizing Inductance[12] (or Air Gap Inductance [7]), $L_{m,1ph}$, and the remaining flux can be attributed to the Leakage Inductance L_l;

$$L_s = L_l + L_{m,1ph}. \tag{32}$$

The apparent inductance per phase is generally higher than the Self Inductance during three phase operation, due to linkage between the phases. Using the relation $i_a + i_b + i_c = 0$, currents in phases B and C can be expressed by the current in phase A, allowing phase A voltage to be expressed as

$$\begin{aligned} E_a =& V_a + j\omega L_s I_a + j\omega M I_b + j\omega M I_c \\ =& V_a + j\omega L_s I_a + j\omega M(I_b + I_c) \\ =& V_a + j\omega(L_s - M)I_a \\ =& V_a + j\omega L I_a, \end{aligned} \tag{33}$$

from which the Synchronous Inductance L is related to the Self- and Mutual Inductances by

$$L = L_s - M \tag{34}$$

1) Analytical Expressions: Developing analytical inductance expressions can be approached in many ways, generally resulting in similar expressions. The following derivation, based on similar methods in [12], assumes an Ideal Doubly Cylindrical Machine[10] (rotor and stator are cylinders), and that the winding is a concentrated Single Layer Winding, i.e. there is only one coil belonging to the same phase per pole, which is equivalent to $q = 1$. All coils are connected in series and have full pitch, yielding an air gap flux resembling a square wave when exciting one phase at a time.

An expression for the Single Phase Magnetizing Inductance $L_{m,1ph}$, can be found by starting out with an expression for the magnetomotive force set up by a coil in a winding with a given current, then calculating the resulting flux through the total winding by assuming that the reluctance of the iron parts is negligible compared to the air gap reluctance:

$$\begin{aligned} mmf = N_{t,coil} I = \frac{2}{p} N_t I = 2l_g H = \frac{2l_g B}{\mu_0} = \frac{2l_g \Phi_{coil}}{\mu_0 A} \\ = \frac{2l_g}{\mu_0 \left(\frac{2\pi Rl}{p}\right)} \cdot \frac{\Psi_{coil}}{N_{t,coil}} = \frac{l_g p}{\mu_0 \pi R l} \cdot \frac{\Psi_{wind}}{N_t} \end{aligned}$$

where $N_{t,coil}$ is the number of turns in one coil and N_t is the total number of series connected turns in the winding, which gives the relation $N_{t,coil} = \frac{2}{p} N_t$ when all coils are connected in series and $q = 1$. Φ_{coil} is the flux through one coil, Ψ_{coil} is the flux linking one coil and Ψ is the flux linking the whole winding. From this the inductance is found by solving for total flux linkage (Ψ), and relating to inductance:

$$L_{m,1ph} = \frac{\Psi}{I} = 2\pi \frac{\mu_0 R l}{l_g} \left(\frac{N_t}{p}\right)^2. \tag{35}$$

Hanselman [7] and Lipo [10] present the same expression, and in addition relates the Mutual Inductance to Single Phase Magnetizing Inductance[1], with the same presumptions, by

$$M = -\frac{1}{3} L_{m,1ph}. \tag{36}$$

For a winding where $q \neq 1$, or the coils are not full pitch, Pyrhönen et al. [14] proposes a slightly different expression, which assumes a sinusoidal flux distribution in the air gap:

$$L_{m,1ph} = \frac{16}{\pi} \cdot \frac{\mu_0 R l}{l_g} \left(\frac{N_t k_w}{p} \right)^2. \tag{37}$$

The expression is essentially the same, only multiplied by $\frac{16}{\pi} \cdot \frac{1}{2\pi} \approx 0.81$, and with the winding factor k_w introduced. To find the Three Phase Magnetizing Inductance, this value is multiplied by $\frac{3}{2}$,

$$L_{m,3ph} = \frac{3}{2} \cdot \frac{16}{\pi} \cdot \frac{\mu_0 R l}{l_g} \left(\frac{N_t k_w}{p} \right)^2. \tag{38}$$

This more closely resembles the inductance of a distributed winding, where the air gap flux approaches a trapezoidal wave as the number of slots increases relative to the number of poles [10] (which is more similar to a sinusoidal wave than a square wave).

2) The Energy Method: The fields resulting from a FEM simulation can be used to calculate the reactances of the machine. If a stationary simulation is performed with the flux remanence of the PMs set to zero, the total magnetic energy can be found and equated to circuit equations describing energy stored in inductors [2]. The relation is as follows:

$$\begin{aligned} W_m =& \frac{1}{2} L_s i_a^2 + \frac{1}{2} L_s i_b^2 + \frac{1}{2} L_s i_c^2 + \\ &+ M i_a i_b + M i_a i_c + M i_b i_c \\ =& \frac{1}{2} i_a \left(L_s i_a + M(i_b + i_c) \right) + \\ &+ \frac{1}{2} i_b \left(L_s i_b + M(i_a + i_c) \right) + \\ &+ \frac{1}{2} i_c \left(L_s i_c + M(i_a + i_b) \right) \\ =& \frac{1}{2} i_a^2 (L_s - M) + \frac{1}{2} i_b^2 (L_s - M) + \frac{1}{2} i_c^2 (L_s - M) \\ =& \frac{1}{2} (i_a^2 + i_b^2 + i_c^2)(L_s - M) \\ =& \frac{1}{2} \cdot \frac{3}{2} \hat{I}^2 L. \end{aligned} \tag{39}$$

The equality can then be solved for the synchronous inductance L, taking mutual linking between phases under three phase operation into account.

The procedure is also valid for machines with Salient Poles or Inset PMs, where the d- and q-axis reactances differ; two stationary simulations are be performed, one with the flux along the d-axis and the other along the q-axis, and the equation is applied twice, resulting in the two respective inductances.

[1]The expression is given only as the magnitude in Hanselman [7], i.e. without the minus sign.

III. The Model

The theory presented in previous sections is utilized when setting up the geometry, the physical relations, the solution sequence and the processing of results for the FEM model.

When constructing the parametric model, two main concerns are kept in mind; it needs to be complex enough to be able to resemble a wide range of machines, and it must be simple enough to be robust and easy to set up. By robust is meant that the geometry and the mesh are built properly, and that the physical relations are applied to the right points, boundaries and domains, for any given set of parameters.

For a static model this is straight forward as the geometric entities to which each physical relation is to be applied can be specified explicitly. However, for the dynamic, parametrized model developed here this is more of a challenge, for instance applying flux remanence in different directions for positive and negative PMs, assigning different currents to coils belonging to different phases, applying symmetry boundary conditions to the right boundaries when supposed to, and so on. This can be done by assigning geometric entities to specific selections when creating them, or by defining selections collecting all geometric entities fulfilling a specific criterion (inside ball or box, adjacent to entity, complementary selection, etc.). The proper physical relations can then be applied to these dynamic selections. Most of the selections are defined by rules applied to the finalized geometry, described in subsection III-B, except for Conductors, PMs and the Sector Symmetry Boundaries, which are defined within the geometry sequence, discussed below.

The complete FEM problem formulation, solution and processing of results are set up in `COMSOL` by the following steps:

- A geometry sequence is defined, which builds the geometry of the model based on a comprehensive list of parameters.
- A number of selections are defined, corresponding to different parts of the machine where particular physical relations, mesh operations etc. are to be applied.
- The proper physical relations are applied to different selections, and material properties are specified.
- Variables are defined, which can be utilized in the simulation or shown as results. Integrations are defined for the variables requiring this, for instance over the region where Arkkio's method is applied.
- A mesh is built, dividing the geometry into elements and nodes, where the element density can be specified.
- The simulation is performed, stationarily or in time.
- The desired results are derived from the FEM-solution.

The steps are described in the same order in the subsequent sections.

A. The Geometry Sequence

The geometry is constructed by combining simple geometric shapes like circles, squares or general polygons in different ways. The intersections, differences and unions of these result in new shapes, on which operations like rotation, mirroring

and copying can be applied. Ultimately the resulting shapes resemble different parts of the machine being modeled. The shapes and operations are specified in a sequence, where all settings of the different features can be specified as functions of globally defined parameters.

For most of the geometry this is trivial, except for some cases discussed below, where special attention is required to ensure the right selections are created and that the geometry is built correctly.

1) Sequence Variation: Some geometry variations require parts of the geometry sequence to be enabled or disabled. For instance, in cases where simulation results are independent of PMs, some parts of the sequence should be disabled, providing a simplified geometry for which a simpler mesh can be built. Similarly, symmetric models require parts of the model to be cut away, which should not be cut away for non-symmetric models.

Rather than manually enabling or disabling parts of the sequence, this is achieved by using if-statements within the sequence that alters it automatically, based on globally defined parameters acting as booleans. The booleans are assigned values equal to one or zero, corresponding to activation or deactivation of sequence parts that, for instance, draw PMs or conductors, or cut away symmetry sectors.

2) PMs: The positive and negative PMs are constructed separately in order to assign them to two different selections. The first positive PM is created, then rotated around the stator at p equally spaced angular positions. All entities resulting from this operation are assigned to a selection by checking the *Contribute to* in the settings of the rotation feature. Similarly, the negative PMs are created and assigned to another selection.

3) Winding Layout: The winding is constructed, similarly to the PMs, by drawing the cross section of one Initial Coil and then copying and rotating it to different angular positions around the stator, assigning the resulting domains to the proper selections according to the winding layout.

The cross section of the Initial Coil depends on the coil span, the extent to which the conductors fill the slots, and whether the winding is a Single Layer- or a Double Layer Winding. If a Single Layer Winding is to be drawn, the two conductors of the Initial Coil occupy a specified share of the complete slot. If a Double Layer Winding is to be drawn, the conductors occupy a specified share of half the area of the complete slot, such that the first conductor lies in the first layer and the return conductor lies in the second layer. The layer division is such that the first layer fills the upper area of the slots, and the second layer fills the area at the bottom, where the divide is placed such as to ensure that both conductors have the same area.

The winding layout is specified in the parameters list as six vectors, one for each phase and polarity. Each vector contains all the slots where coils are to be placed and connected for that phase-polarity.

The first of the conductors of the Initial Coil is rotated around the stator (without being removed) in six operations, one for each phase-polarity, filling the slots determined by the corresponding vector. The entities resulting from these rotations are then set to *Contribute to* their respective selections (A^+, A^-, B^+...).The same rotation procedure is carried out with the other conductor of the Initial Coil, but assigning the resulting entities to selections corresponding to the opposite polarity, as these conductors carry the current in the opposite direction. Finally, the conductors of the Initial Coil are removed from the geometry.

Initial Coil is drawn	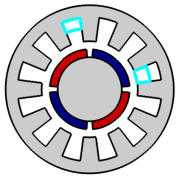	
First conductors of positive polarity coils belonging to phase A is drawn	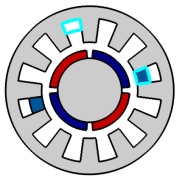	Contribute to selection A+
First conductors of negative polarity coils belonging to phase A is drawn	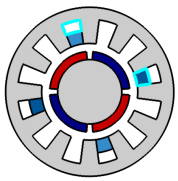	Contribute to selection A-
Return conductors of positive polarity coils belonging to phase A is drawn	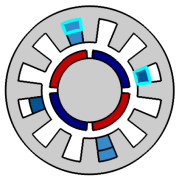	Contribute to selection A-
Return conductors of negative polarity coils belonging to phase A is drawn	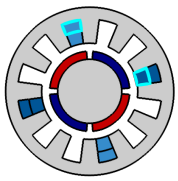	Contribute to selection A+

Table I: Constructing the Winding, shown for phase A in a 4p, 12S Double Layer Winding. The vectors corresponding to positive and negative polarity coils belonging to phase A are given by $[1, 7]$ and $[4, 0]$, respectively.

This results in six selections, each containing a number of conductors which, if the coils of the respective phases were to be connected in series and fed a current, would carry the same current in the same direction.

The procedure is shown for phase A in a 4p, 12S winding in Table I.

4) Symmetry: For a periodic model, only a fraction of the complete machine needs to be modeled. This is achieved by cutting away superfluous sectors at the end of the geometry sequence, arriving at a finalized geometry spanning an angle

of

$$\gamma = \frac{2\pi}{N_{rep}}$$

above the x-axis. The new boundaries in the circumferential direction needs to be assigned periodic conditions, and therefore should be collected in selections. The boundary in the clockwise (CW) direction lies along the positive x-axis, while the boundary in the counterclockwise (CCW) direction lies along an axis γ CCW of the x-axis, with the center of the machine in origo. The CW boundaries can then be collected by selecting all boundaries along or below the x-axis. This is done in practice by defining a box selection, assigning all boundaries inside the box given by

$$0 \leq x \leq \infty$$
$$-\infty \leq y \leq 0$$

to the same selection.

Box selections can only be defined as rectangles with constant x- or y-values along the sides. Therefore, to assign the CCW sector boundaries to another selection, the whole geometry is rotated an angle $-\gamma$, such that the CCW boundaries lie along the x-axis. Then a new box selection can be defined to collect all the boundaries along or above the x-axis to a new selection, with the box given by

$$0 \leq x \leq \infty$$
$$0 \leq y \leq \infty,$$

before the whole geometry is rotated back again.

5) Air gap: The boundary between the rotating and the stationary regions is positioned in the middle of the air gap. To apply Arkkio's Method for torque calculation, presented in subsection II-F, a cylindrical region is defined on both sides of the boundary.

6) The Machine Assembly: The rotating and stationary regions are created as two separate objects, such that the inner boundary of the stationary region is not the same as the outer boundary of the rotating region, although they are overlapping. At the end of the geometry sequence the option *Form an assembly* is selected, which ensures that the two regions are not merged into one object. By checking the option *Create Identity Pairs*, a pair consisting of the two boundaries is created, on which specific boundary conditions can be applied to ensure continuity between the two regions.

B. Selections

The assignment of boundaries and domains to selections for PMs, Conductors and circumferential Sector Symmetry Boundaries happens within the geometry sequence, as described above.

However, a whole range of selections must still be defined to ensure that all physical relations are applied to the right geometric entities, for the mesh to build, and for the results to show properly. These are defined on the finalized geometry, which can be done either at the end of the geometry sequence or in *Definitions*. The numerous other selections are not discussed in detail, rather the general way of thinking is outlined:

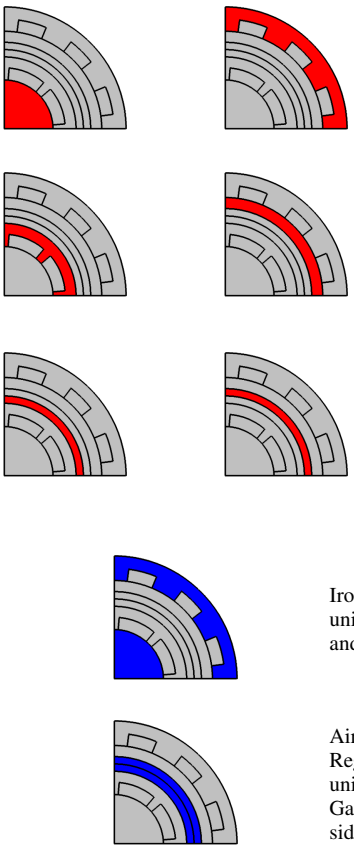

Table II: Defining Selections

The remaining selections are defined by starting out with defining the Rotor Core and Stator Core selections, which are easily collected by using a ball selection and a box selection. Then new selections are defined to collect all domains or boundaries adjacent to some other predefined selection. By working inwards from the Rotor and Stator Core, all domains can be reached this way. The process is shown in Table II.

The final selections to be utilized for applying physical relations can then be defined as unions, intersections and differences of these, as shown for Iron and the Air Gap Boundary Region.

C. Physical Relations

The equations and boundary conditions of the FEM-problem, resembling the physical laws acting in the machine, are applied using the *Rotating Machinery, Magnetic* module. This module makes it straight forward to apply relations describing rotation of the rotor, continuity between the rotating and the stationary region, sector symmetries and more.

1) Flux remanence of PMs: The positive and negative PMs are assigned their remanent flux densities with *Ampère's Law* relations, one for each polarity. A cylindrical coordinate system is defined in *Definitions*, allowing the remanence to be specified in the radial direction.

2) Current Excitation: The machine is excited by specifying a current in the three phases. It is applied using an *External Current Density* feature, one for each of the six phase-polarities. The magnitude of the current density is specified in the z-direction as

$$J = \frac{N_{t,coil} I_a}{N_{par} A_c} \tag{40}$$

for conductors in the selection *A+*, and similarly for the other phase-polarities. $N_{t,coil}$ is the number of turns in one coil, A_c is the area of the cross section of one conductor of a coil, and N_{par} is the number of parallel connections in each phase.

3) Rotor Rotation: The rotation of the rotor and the air gap region surrounding it is specified with a *Prescribed Rotation* feature, readily available in the *Rotating Machinery, Magnetic* module.

4) Continuity: The continuity between the rotating and stationary regions is achieved by applying a *Continuity* boundary condition on the *Identity Pair* mentioned in subsection III-A. If symmetry is being utilized in the simulation, this feature is replaced by a similar condition, mentioned below.

5) Sector Symmetry and Periodic Conditions: If symmetry is being utilized, the *Sector Symmetry* condition is applied on the *Identity Pair* with the desired periodicity (anti-periodic or periodic) and number of symmetry sectors, where the maximum is 50 sectors. In addition, two *Periodic Conditions* are applied to the sector symmetry boundaries in the circumferential direction, one for the rotating region and another for the stationary region. These are equipped with a *Destination Selection*, where either the boundaries in clockwise or counterclockwise direction are specified, to ensure information flows from and to the right boundaries.

It is found that the *Sector Symmetry* and *Periodic Conditions* generally should be specified with the same periodicity. However, an exception is found for the case when there is only two symmetry sectors; it is found that for this particular case the *Periodic Conditions* should be opposite of the *Sector Symmetry* feature.

6) Materials: The different regions are assigned standard, built in materials. The air gap, PMs and conductors are set to behave as *Air*, while the stator and rotor core are assigned the material properties of *Soft Iron (without losses)*. The latter material is in addition assigned a relative permeability of 1000.

The material *Soft Iron* comes with an interpolation curve describing a non-linear relation between the B and H-fields, which allows saturation to be modeled. This is not taken into account here, but could easily be included in the model by specifying a separate *Ampère's Law* relation for the iron parts, with the *Constitutive Relation*-setting for *Magnetic Field* set to *BH-curve*.

The material choice for conductors is arbitrary, as the *External Current Density*-feature causes the conductors to carry the specified current regardless of material properties.

D. Variable Definitions

Variables are defined to be utilized in physical relations, or to be shown in results. The three phase currents are defined and utilized in the *External Current Density*-features, the rotor angle in *Prescribed Rotation*.

Phase voltages are calculated according to Equation 21. The equation is slightly modified to take the effect of parallel connections into account. Also, the integration is performed over all areas corresponding to cross sections of all conductors belonging to the same phase, with the opposite polarities added with opposite sign. The six integrations are defined in *Definitions*, one for each of the six selections containing conductors carrying the same current. The resulting expression is

$$V_a = \frac{N_{t,coil} l}{N_{par} A_c} \cdot \left[\int_{S_{\mathrm{A}+}} E_z \, \mathrm{d}S - \int_{S_{\mathrm{A}-}} E_z \, \mathrm{d}S \right] \tag{41}$$

In addition, the whole expression is multiplied by a "symmetry compensation" parameter, which assumes the value 1 for a non-symmetric model, yielding no difference, and the value N_{rep} for a symmetric model.

To be able to display voltage in a phasor diagram, the equations of the fundamental Fourier Series coefficients are specified as variables, according to equations in subsection II-G. Integrations are performed in time, and then used to derive magnitude and angle of the voltage phasor.

Torque is calculated according to Equation 14, also requiring an integration to be defined on the regions on each side of the air gap. This expression is also multiplied by the same symmetry compensation parameter.

E. Mesh

The accuracy of the solution increases with the element density of the mesh. However, this also implies increasing the degrees of freedom, resulting in memory demanding, time consuming computations. The mesh for this model is constructed in an attempt to satisfy both concerns, allowing a dense mesh, for instance when assessing cogging torque in a fractional slot machine, and a coarse mesh, for a quick and approximate solution.

The ability of the mesh to a produce a solution with a low error can be measured by looking at the Element Quality of individual elements. This measure is highly dependent on the shape of the element in question; elements where the sides are roughly the same length, and the angles are neither very small or very large, i.e. elements resembling rectangles and equilateral triangles, are associated with higher quality. This allows the quality of the complete mesh to be measured by the Average Element Quality or the Minimum Element Quality.

The order in which the different regions of the geometry are meshed is essential to achieve a good mesh quality. For instance, if the first regions to be meshed were those representing the PMs, these simple shapes would not require a high element density, resulting in a coarse distribution along the PM edges. However, a thin air gap would require a high element density along the PM edges to keep the element quality at a reasonable level. The more complex air gap region should therefore be meshed before the simpler PM regions.

The first regions to be meshed in the sequence implemented here are the regions on both sides of the boundary between the stationary and rotating regions, where Arkkio's Method is applied. This region is meshed with quadratic elements, resulting from distributing a set number of edge elements in the radial and circumferential directions, and mapping these over the domain. This provides some control of the density in this essential region, and ensures at least three boundary layers between the rotor and stator, which can be regarded a rule of thumb [14] for achieving good results. The effect of increasing the number of boundary layers is indicated in Figure 3.

Next, the rest of the air gap is meshed with a specified element density. Generally, this region has a higher element density than the other regions. Then the PMs and conductors are meshed, and finally, the stator and rotor cores.

For models where symmetry is applied, special attention should be payed to the resulting sector symmetry boundaries in the circumferential directions. To minimize the discontinuity in the information flowing between these boundaries, the clockwise (CW) or counterclockwise (CCW) boundary could be meshed before the interior domains, and then copied on to the other side. However, this would not take into account that, for instance, the PMs might be positioned such that their circumferential boundary would come very close to the sector symmetry boundary, requiring the air gap domain to be meshed before the sector symmetry boundary, similarly to the case described above, to arrive at a decent mesh quality. For this reason, the discontinuity between the CW and CCW symmetry sector boundaries is instead minimized by increasing the element density along these edges.

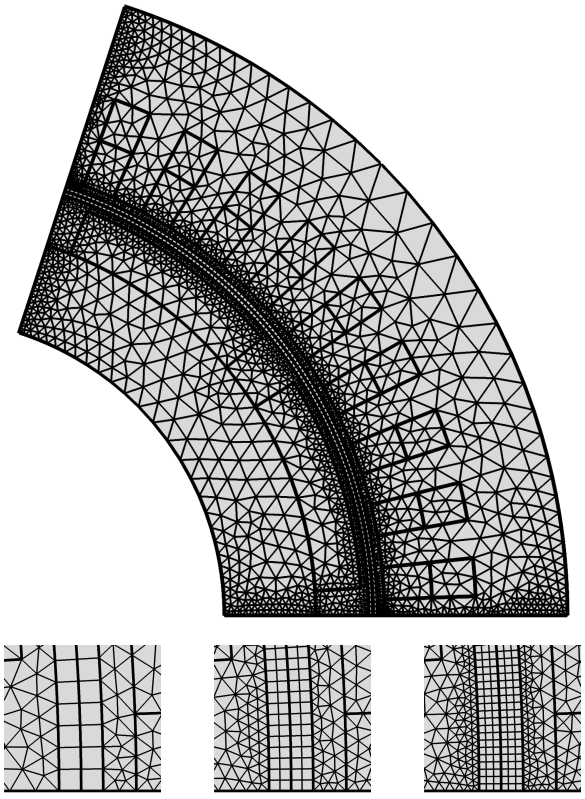

(a) 1 layers (b) 2 layers (c) 3 layers

Figure 3: Mesh sample for 10p, 45S Machine. The smaller figures indicate the effect of increasing the number of boundary layers on each side of the stator/rotor boundary. The relative thickness of the boundary region is 0.4.

F. Simulation

The study types to be conducted here are *Stationary*, *Time Dependent*, *Parametric Stationary* and *Parametric Time Dependent*. These are defined as four separate studies, rather than defining only one study and activating/deactivating time dependence and parametric iteration, as this appears to provide easier, more predictable solution handling.

1) Stationary: The Stationary Study is straight forward to define, and needs no particular settings to be set to run properly. However, to avoid errors concerning time dependent variables (currents, rotor rotation, etc), a parameter $t = 0$ is defined in the parameters list, so that the mentioned variables do not have to be deactivated for the stationary study to run properly.

2) Time Dependent: The default Time Dependent Study is altered such that the maximum step size that the solver takes is no larger than the time between two stored time instants. This is because variables on some occurrences update only at the steps taken by the solver, thus producing an unsmooth output. The solver is set to store a number of time instants, ranging from 0 to a specified ending time. Time dependency of variables is achieved by stating them as a function of t.

3) Parametric Studies: A Parametric Sweep feature is added to similar Stationary and Time Dependent Studies as defined above. The values in a specified array are assigned to the sweep variable u successively. The other model parameters can then be set to depend on u.

In the Parametric Sweep feature, the setting *Use parametric solver* is deactivated. This is to ensure that the solver does not attempt to store the solution in a more efficient way, which needs to be handled differently to access sub-solutions corresponding to different values of the sweep variable.

G. Post-Processing

All the results that are to be viewed from the Application must be defined within the model on forehand. *2D Surface Plot*s are defined showing magnetic flux density, the z-component of the vector potential and the z-component of current density. If a simulation was performed on a sector of a periodic machine, all the symmetric sectors can be viewed by defining a *Sector 2D*-data set, and selecting this as input of the 2D plots. The number of symmetric sectors must be specified in the settings of the sector-data set, and if the solution is anti-periodic, this is accounted for by selecting *Invert phase when rotating* under advanced settings.

An *1D Line Plot* is defined to show air gap flux density, a *1D Table Plot* is defined to show results from derived values,

and a plot to show phasors is defined as a *2D Arrow Surface Plot*. The settings of all the plots are largely controlled from the Application.

IV. The Application Builder

Using the embedded *Application Builder* in COMSOL a GUI is built, with the goal of allowing quick and easy control of geometry, simulation conditions and post-processing described in section III.

A. User Interaction

A lot of thought can be put into the matter of how the Application should interact with the user, specifically how geometrical parameters and simulation conditions are specified, and how results are displayed.

Depending on which characteristics of a machine are being assessed, the simulations to be performed are quite different: Inductances requires only a stationary study, cogging torque assessment requires a time dependent study, a torque characteristic might require a parametric, time dependent study. The different study types are relatively straight forward to set up in the simulation section, but when presenting results this becomes somewhat more complicated.

For a reasonably user friendly experience, the Application should display only results and result handling tools that actually make sense for that particular solution. First, this requires the Application to differentiate between stationary, time dependent and parametric studies: For instance, a Fourier transform should only be available in the case of a time dependent or parametric study, and buttons for navigating through time instants should only be shown for a time dependent study, and so on. Second, some results only make sense for particular simulation conditions: For instance, applying the Energy Method to calculate inductances does not make much sense when the flux remanence of PMs is nonzero. Also, for the case of a cylindrical rotor, both the internal generated voltage and the synchronous reactance could be calculated for any time dependent simulation by using Equation 18 and Equation 19, but not for the case when the current was directed along the q-axis.

The results section therefore needs to adapt to the solution being viewed. Regarding results handling tools, this is relatively straight forward, as they mainly depend on which of the four study types was conducted (stationary, time dependent, parametric stationary or parametric time dependent). Regarding whether or not to show different results, this mainly concerns inductances at this state of development of the Application. When using the Energy Method, the user is informed that the result is only valid after a certain simulation preset was ran. Regarding Equation 18 and Equation 19, these are utilized in a routine that calculates the inductances automatically, which is accessible only after another specific preset is run.

The point of this short discussion is simply to emphasize that as the Application gets more advanced and new result types are added, then these need to be incorporated into the Application and presented in an instructive way; this is generally required to be quite well thought through to arrive at a reasonably user friendly experience.

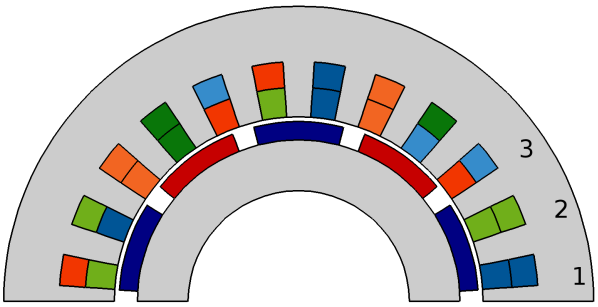

Figure 4: Sample of how the geometry of the model is displayed. Dark and light shade of blue correspond to phase A conductors in positive and negative z-direction. Similarly, red and green correspond to phases B and C.

B. Layout and Functionality

The layout of the GUI is basically comprised of three main panes for user input (geometry, simulation and results), and a graphics window, displaying geometry, meshes and results. In addition there are two main buttons, *Build* and *Compute*, two buttons for saving an instance of the application with current results and input parameters, and an information display.

The build button draws the geometry of the motor based on the current input parameters. For clarity the non-physical stator/rotor-boundaries in the air gap are hidden. The PMs are colored dark red and blue, describing negative- and positive polarity, and the conductors of the winding are colored blue, red and green in two shades, describing to which phase the conductors belong, and in which polarity they are connected. An example of a 10p, 24S-motor is shown in figure Figure 4, with the same winding arrangement as shown in Figure 1.

Before the geometry builds a method is always run to check whether the specified geometry parameters will result in a valid geometry. This is found to be necessary, as an erroneous input in some instances causes a corrupted geometry sequence that must be fixed from within the Model. The method verifies that that the number of poles is an even number above zero, that the number of slots is greater than two, and that the radial dimensions are compatible with each other, i.e. the rotor radius is smaller than the stator radius, the PMs don't touch the stator, etc. An instructive error is shown if this is not the case.

When the *Compute*-button is pressed, the simulation starts. The Application allows results to be viewed while the solver is working on a Parametric or Time Dependent Study, but due to what appears to be a bug in the program, the *Zoom Extents*-button in the Graphics-pane must be pressed after simulation has started in order for this to work.

1) Geometry: In this pane the geometry of the motor is constructed, the winding layout is conducted, symmetry conditions are applied and a mesh is built. When this pane is

being shown, the information display shows the value of q, the winding factor and angle, whether the winding is symmetric or not, and the number of elements and the minimum element quality of the mesh.

Predefined Motors A predefined parameter set can be loaded, resembling a specific machine. All the example simulations described in section VI are stored here.

Poles/Slots The number of poles and slots of the machine are specified. The resulting value of q is also calculated, according to Equation 4, and displayed for this particular combination.

Dimensions Main geometrical dimensions are specified as inner and outer stator and rotor radiuses, stator slot width and depth, and axial length.

Winding The winding is categorized as of either double layer or single layer type, and the phases are set to occupy the slots around the stator according to a winding layout, which is either specified manually or automatically according to theory described in subsection II-D. The choices are also available to adjust the extent to which the conductors fill the slots in the stator in the radial and circumferential directions, and to disable the winding, for instance if no load-conditions are to be simulated. When the winding layout is performed the winding factor and angle are calculated, according to Equation 12 and Equation 13, and shown in the information display to give an indicator of the expected performance of the winding. The latter is also made available when choosing the offset angle with which the current is to be applied, described below.

PM The radial position, the relative width and the height of the PMs are specified, as well as their remanent flux density. The option is also available to disable the PMs, in case for instance reactance calculations are performed using the Energy Method.

Symmetry Whether or not to take advantage of periodicity in calculations is specified, as well as the number of sectors and the type of periodicity. An auto setting is available, choosing the highest possible number of symmetries. When symmetry is activated, a method is run that activates *Sector Symmetry* and deactivates *Continuity* in the model, and the correct periodic/anti-periodic setting is set in *Sector Symmetry* and both *Periodic Conditions*. The *Periodic Conditions* don't need to be deactivated, as the boundary selections to which they are applied are empty.

Mesh The relative thickness of the region where Arkkio's Method is applied is specified as a fraction of the minimum length of the air gap. Along with the number of radial boundary layers on each side of the stator/rotor boundary, this determines the number of quadratic elements in the circumferential direction. The element density of the remaining parts of the mesh is specified as one out of nine grades, ranging from dense to coarse, directed at three different geometric selections; the remaining air gap, the circumferential sector symmetry boundaries (if symmetry is activated) and the remaining geometry. When the mesh is built, the number of elements that the mesh consists of is shown in the information display, along with the minimum element quality, giving an impression of the magnitude of the problem to be solved and the quality of the mesh. A quality plot is also available, which displays the mesh with elements colored corresponding to their quality, indicating where the element density should be increased to improve the mesh.

2) Simulation: In this pane the conditions under which the model is to be simulated are specified. The information display shows the current study type (time dependent, parametric etc.), the number of time instants and parameter sweep values to be computed and stored, and the amplitude of the current and resulting current density.

Parametric Study If a parametric study is chosen, the values that are to be assigned to the parameter u for each iteration is specified as an array. The user input in almost all fields in the geometry and simulation panes, except the number of symmetry sectors and the number of time instants to be stored, can be a function of u, which makes it straight forward to conduct a study of how the properties of the machine changes with a geometric parameter, or how a machine performs under different conditions. One important restriction when performing a parametric study is that methods in the application will not be run between iterations of the study. This means that if, for instance, the number of slots is entered as a function of u, then a new winding layout will not be performed on each iteration, even though the automatic winding layout setting is active. Similarly, the sector symmetry settings will not be updated between iterations.

Time Dependent Study If a time dependent study is chosen, the study will be conducted in time, ending at the specified simulation time, and the specified number of equally spaced time instants will be stored. Time dependent variables are specified as functions of t.

Rotor Angle The angular velocity of the rotor and the initial displacement is specified, where the default velocity is that which makes the rotor rotate in synchronism with the electric field produced by the stator, $\omega_m = \frac{2\omega}{p}$. If desired another expression than the default, describing constant angular velocity, can be specified, for instance during single phase excitation when performing reactance calculations, where the rotor stands still.

Currents The currents are specified with an amplitude, a frequency, and an offset angle. There is also an option for relating the current to the spatial d-axis and q-axis, based on the angle of the winding, discussed in subsection II-D. If desired, other equations than those describing symmetric three phase currents can be specified.

Preset Studies A range of preset studies can be chosen, setting the above simulation parameters to appropriate values:

- No Load, Electrical Period: Time dependent study, one electrical cycle is simulated. Current is zero.
- No Load, Cogging Torque Cycle: Time dependent study, one cogging torque cycle is simulated, according to Equation 16. Current is zero.
- Load, Generator Operation: Time dependent study, one electrical cycle. Current lagging d-axis by $45°$.
- Load, Motor Operation: Time dependent study, one electrical cycle. Current leading d-axis by $45°$.
- Load, Torque Characteristic: Parametric, time dependent study. One electrical cycle is simulated for current angles ranging between $180°$ lagging and $180°$ leading d-axis, allowing a torque characteristic to be drawn in the results section by plotting the time-averaged torque as a function of u. To increase the "resolution" of the characteristic, the number of parameter iterations can be increased.
- Load, Torque Characteristic (fast): Parametric, stationary study. Similar to the previous preset, but torque is calculated from stationary simulations only, which is a lot quicker. However, this does not account for torque ripple, possibly causing a biased characteristic if this is significant.
- Reactance Study, Cylindrical Rotor: Stationary study. Current is applied while flux remanence of PMs is zero, allowing the Energy Method to be applied for reactance calculations. Values are plotted by choosing Reactances in Evaluation, mentioned below.
- Reactance Study, d- and q-axis: Parametric, stationary study. Similar to the previous preset, but two simulations are conducted: The first with current in d-axis ($u = 0$), the second with current in q-axis ($u = 1$). This allows the respective d- and q-axis reactances to be calculated.
- Reactance Study, Continuous Variation: Parametric, stationary study. Similar to the two previous presets, but the current angle is varied continuously between $90°$ lagging and $90°$ leading d-axis, allowing the continuous reactance variation to be plotted.
- Single Phase Excitation: Time dependent study, one electrical cycle. Only phase A is excited with a current of $1\,\mathrm{A}$ while the rotor stands still. Single Phase Self- and Mutual Reactances can then be found directly as the amplitude of the respective voltages in phase A and B (or C).

For all reactance and load presets, if no current is specified a current resulting in a current density of $2\,\mathrm{A/mm}$ is applied automatically. For a Load preset, if the flux remanence of PMs is zero (possibly after a reactance study was conducted) the user will be prompted with this before simulation.

3) Results: In this pane the simulation results are processed and displayed. If a time dependent and/or parametric study was conducted, a navigation panel is available in all sub-panes, allowing quick and easy browsing through stored time instants and parametric sweep values of the solution. The results are shown in the graphics display to the right, and can be viewed either one at a time, or all at the same time by activating *Tiled View*, available by pressing the button near the navigation panel. The information display shows the study type being displayed, and the time it took to solve it.

Surface Plots Magnetic flux density, vector potential or current density is plotted for the given solution. If periodicity is utilized in the current solution, the choice is available to show or hide all symmetric sectors. This is performed by a method that changes the data set for all 2D plots to the 2D Sector-set (subsection III-G), and sets the appropriate number of sectors. Also, if the type of periodicity is anti-periodic, the phase is inverted when rotating. An important note in this context is that the current density is not shown properly when inverting the phase, for reasons unknown. However, this is considered a minor flaw, as all other results appear to be unaffected by the introduction of symmetry. A section for generating an animation is available when multiple solutions exist (if time dependent or parametric study was conducted). The number of frames per second is specified, as well as either t or u as variable to be looped over, and the animation is played once in the animation graphics display, or exported as a GIF.

Evaluation A plot quantity is chosen among the available choices: Torque, Current, Voltage, Electrical Power, Mechanical Power, Reactances and Expression. Plotting reactance calculations only gives valid results if the current was non-zero and flux remanence of PMs was zero during simulation. If Expression is chosen, a input field where a custom expression can be specified appears. This allows functions of parameters and result variables within the model to be plotted, which is useful for debugging, and when adding new functionality. Depending on the study type, the chosen quantity is plotted against either time (t), if time dependent, or parameter (u), if parametric, along the x-axis. If a parametric, time dependent study was conducted, either t or u can be chosen along the x-axis. The different solutions corresponding to the other variable can either be plotted one at a time, all together, or a specific operation can be applied: Average, Maximize or Root Mean Square (RMS). For instance, to plot a torque characteristic (from the results of a *Torque Characteristic* preset study), u can be chosen along the x-axis, and the different time instants can be averaged over. Finally, a Fast Fourier Transform can be applied. The plot shows the RMS value of the occurrences of different frequencies in the signal being analyzed, such that the actual amplitudes are found by multiplying by $\sqrt{2}$.If the the signal is being transformed as a function of t, the frequencies along the x-axis are multiples of the electrical frequency in the system. If it is being transformed as a function of u, no frequency scaling is applied.

Air Gap Flux The flux through the air gap is plotted as a func-

tion of the arc length for the given solution. The boundary for which the flux is plotted can be chosen as either one of the two boundaries that connects the stationary and rotating regions, or the inner or outer boundary of the cylindrical region where Arkkio's Method is applied.

Time Averages When a time dependent study was conducted, this section presents a summary of the simulation, displaying the voltage, current, average values of torque, electrical and mechanical power, efficiency, power factor and reactive power. Due to this model being lossless, the calculated efficiency don't make much physical meaning at this point, but is included anyway as an indicator of consistency of the model (indicating the correlation between electrical and mechanical power), and the accuracy of the solution.

Phasor Plots For a stationary study, a phasor representing the current, as well as its d- and q-axis decomposition, is shown. The value of E, X_d and X_q can be specified manually, if known from a previous study, or calculated automatically if a *Parameter Estimation Study* was conducted. If a time dependent study was conducted, a phasor representing voltage is also shown.

C. Implementation

The functionality described in the previous subsection is incorporated into the GUI, which is built by creating *forms* that contain different graphical objects; text, buttons, graphic displays, form collections, etc. Buttons and events might be set to execute simple commands, like changing model parameters and activating or deactivating features, or more complex *methods* written in a Java or C-like syntax, allowing for instance the winding layout routine described in subsection II-D to be implemented.

The Application can be viewed as a program that is separate from the model, but has access to all model parameters, features and results. It has its own set of variables, which are used to control the state of objects, like check boxes, lists and form collections within the application.

Using the Application Builder is relatively straight forward, and basic functionality is not described more closely here. However, some less intuitive parts, requiring more comprehensive programming and workarounds to arrive at the desired functionality, are described below.

1) Displaying the Motor: The ability to display the model in an instructive way is essential, especially in an educational setting. However, the standard geometry view in COMSOL does not allow a lot of flexibility regarding how the model is displayed. Due to this a more customized routine is implemented to display the machine, which perhaps appears somewhat cumbersome, but works quite well and adds only a negligible time delay compared to the standard geometry view.

The post-processing section contains a wider range of display options, allowing annotations and colors to be applied to specific domains. To make the geometry available in the post-processing section without performing a simulation, which takes more time, a quick and simple mesh is built with elements only on the domains and boundaries to be displayed. This allows a *Mesh Plot* to be generated.

The mesh then appears as a data set in the results section. Eight additional mesh data sets are defined, resulting in a total of nine sets, one for each color to be displayed in the machine (positive/negative PMs, six phase-polarities, and iron). All the nine data sets have the same input mesh, but by applying a *Selection* feature, only the selected domains are shown when plotting the data set.

The nine different domains can now be plotted in a surface plot with different colors and annotations, yielding the display shown in Figure 4.

2) Solution Handling: To present the range of sub-solutions resulting from a time dependent and/or parametric study, the corresponding time instants and parameter values are loaded into the application as arrays from the current solution. These two arrays are used to display the different time instants and parameter values in the application, as well as to ensure that no attempt is made to access sub-solutions that do not exist. Also, to be able to display all the symmetry sectors from a symmetric solution properly, the number of symmetry sectors and the type of periodicity must be known.

All the necessary results-handling variables are collected from the solution by a method that is called on startup and when a new solution is computed.

The method also detects the type of study of the current solution. Some result handling tools (animations, Fourier Transform, navigating through time instants and parametric sweep variables) are activated or deactivated depending on this: For instance, all the buttons and input fields related to generating an animation are stored within a *Card Stack*, which is a default object in the *Application Builder*. The card stack displays different "cards" depending on the value of some input variable, in this case a string assuming values corresponding to the current type of solution. The card containing animation-related objects is displayed only for a parametric or time dependent study, while an empty card is displayed otherwise.

3) Winding Layout: The winding layout is displayed and edited in a table which consists of three columns; the first contains the slot numbering, the second contains the first conductor of each coil, and the third contains the return conductor of each coil. Only the second column is editable, as the third is determined by the coil span. Letters with signs corresponding to phases and polarities are entered by the user (A^+, A^-, B^+...), and then interpreted and applied into the model as vectors containing slots to be occupied by the respective phases.

This is performed by a "winding update"'-method that is called every time the winding is edited, or when the number of poles or slots change. In addition to this, the method calculates the winding factor according to Equation 12, the angle θ_{wind} according to Equation 13, and the possible numbers of parallel connections. If the winding is of single layer type, then entries made in even slots are removed instantaneously.

If automatic winding layout is activated, another method is called to perform the layout of a double layer winding, according to subsection II-D. If the winding is specified to be of single layer type, the winding is converted by the "update" method, which removes every other coil and changes the coil span if necessary.

4) Parameter Estimation: Running a *Parameter Estimation Study* results in two time dependent simulations over one electrical cycle being performed, one under no load and one under load. The former corresponds to $u = 0$, the latter to $u = 1$.

The results from this study contain information that allows the internal generated voltage E and the d- and q-axis reactances, X_d and X_q, to be calculated. Performing this study activates a *Calculate*-button in the pane for phasor plots. Pressing this button executes a method that performs the necessary calculations and enters the result into the input fields for E, X_d and X_q. The routine is as follows:

The magnitude of E is found from the no load case, equal to the fundamental of the terminal voltage, V, calculated using Equation 24. From the load case the voltage and current magnitudes, as well as their angles with respect to the angles of the d- and q-axis, are used to calculate X_d and X_q, according to Equation 18 and Equation 19.

5) Phasor Diagram: Plotting of phasors is another example of functionality that is not straight forward available in COMSOL. Since this is a very instructive tool in describing operation of PM machines, some extra time is spent on finding a work-around that allows phasors to be plotted.

The main idea to achieve this is to define an *Arrow Surface* plot for each phasor to be displayed. The settings of the plots are specified such as to draw only one arrow in one specific coordinate, where the x- and y-components of the arrow is given by decomposition of currents and voltages along the x- and y-axis.

The arrow plots are controlled from the application to make sure they are scaled appropriately with respect to each other. The current is plotted with a magnitude of one, with the d- and q-axis components scaled after this. If no internal generated voltage is specified (in the input field), the induced voltage is plotted with magnitude one. If internal generated voltage is specified, this voltage is plotted with magnitude one, and the other voltages are scaled with respect to it.

V. Validation of The Model

The Application described in the preceding sections is able to initialize and perform a range of different studies. This section is devoted to assess whether the results produced from these studies are valid. Three ways in which validity of the results can be indicated are as follows:

1) The output can quickly be declared invalid if it clearly breaks basic physical laws.
2) Parameters and characteristics produced by the model can be compared to analytical formulas.
3) Other studies with known input parameters and results can be recreated and compared to the output of the model.

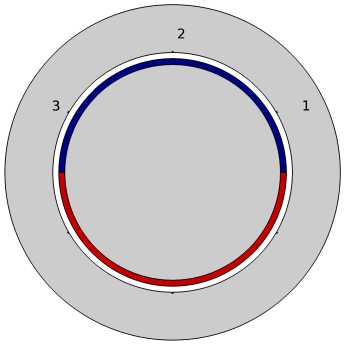

L	100 mm
$R_{s,out}$	140 mm
$R_{s,in}$	100 mm
$R_{r,out}$	90 mm
$R_{r,in}$	0 mm
p	2
Q	6
S_d	1 mm
S_w	0.01
R_{PM}	90 mm
PM_h	5 mm
PM_w	1
PM_{br}	1 T
$N_{t,coil}$	50
N_{par}	1

Figure 5: Model of Ideal Doubly Cylindrical Machine for comparison with analytical expressions.

The first point could concern, for instance, conservation of energy: For this lossless system, this would be analogous to the average energy produced/consumed by the machine equaling the mechanical energy consumed/produced. For time dependent studies this is verified by calculating the electrical power from phase voltages and currents, and comparing it to the mechanical power, calculated from torque and rotational speed. It is found that these are essentially equal in all time dependent studies presented in the following sections. This is a good indicator of consistency of results, as these quantities are calculated from quite different output data of the model; the voltages by integrating the electric field intensity $\mathbf{E}$ in the conductors, torque by integrating the magnetic field in the air gap.

Regarding validation by comparing to analytical formulas, this is performed for internal generated voltage and inductances only, as the focus of this work is applying FEM, not dwelling deep into analytical formulas.

Regarding recreation of other studies, two studies are presented where this was fairly successful. However, it should be noted that in other cases the results did not match that well. Due to the numerous other possible causes than this model not producing valid results (for instance typos in input parameters, misinterpretation of parameters, invalid results in the other studies, inaccurate replication of geometry), this is not dwelled more with, and the treatment in the following sections is considered thorough enough to indicate validity of the model.

A. Inductances in an Ideal Doubly Cylindrical Machine

To verify inductance values, a geometry is constructed attempting to meet the presumptions of the analytical formulas in subsection II-J, such that correlation between analytical formulas and simulation results should be good. The PMs are assumed to be surface mounted with relative permeability equal to air. The stator slots are reduced in size, approaching

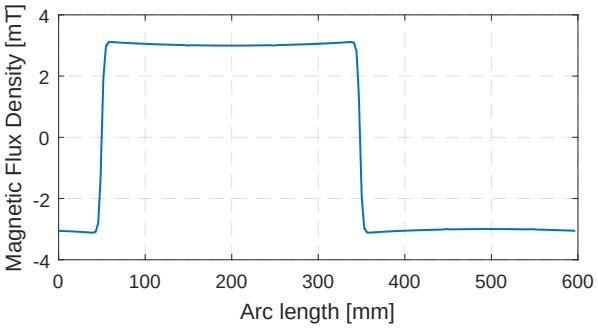

Figure 6: Magnetic flux density along air gap during Single Phase Excitation with PMs deactivated. 2p, 6S machine with Concentrated Single Layer Winding.

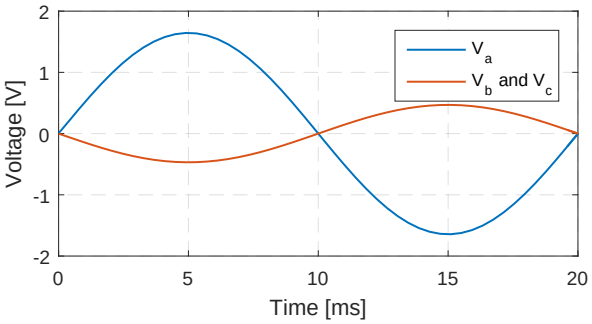

Figure 7: Voltage Induction during Single Phase Excitation in 2p, 6S machine with a Concentrated Single Layer Winding. Only phase A is excited with a current of 1 A.

infinitesimally thin conductors on the inner surface of the stator, yielding a cylindrical stator. The model of the machine and geometrical dimensions is shown in Figure 5.

1) Full Pitch Concentrated Winding: The cylindrical machine is set to have 2 poles and 6 slots, and a single layer winding comprised of 3 full pitch coils. Using Equation 35 and Equation 36, analytical Single Phase Magnetizing- and Mutual Inductances in this machine are found to be

$$L_{m,1ph} = 4.689\,\mathrm{mH}$$
$$M = -1.563\,\mathrm{mH}.$$

To check these values against the model, a simulation is performed with sinusoidal excitation of a single phase only. The resulting air gap flux is shown in Figure 6. This distribution resembles a square wave quite well, which is a prerequisite in Equation 35 and Equation 36. From voltages induced in phases, shown in Figure 7, the Self- and Mutual Reactances can be read directly as the voltage amplitude (due to an excitation current of 1 A), corresponding to inductance values below (frequency is 50 Hz). Using the Energy Method to calculate the Self Inductance in this situation gives the exact same value.

$$L_s = 5.230\,\mathrm{mH}$$

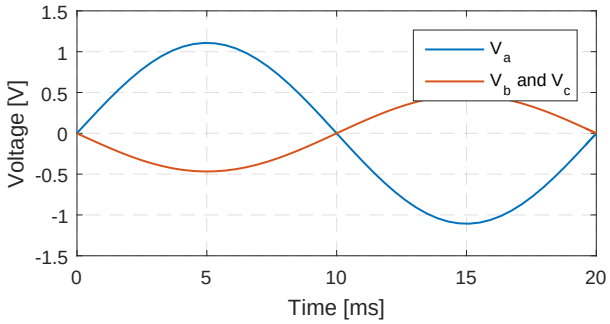

Figure 8: Voltage Induction during Single Phase Excitation in 2p, 180S machine with a Concentrated Single Layer Winding. Only phase A is excited with a current of 1 A.

$$M = -1.489\,\mathrm{mH}.$$

The Self Inductance is somewhat higher than the analytical Single Phase Magnetizing Inductance, due to only the latter incorporating Leakage Inductance. The values for Mutual Inductance resemble each other more closely. The slightly higher analytical value could be caused by a non-zero reluctance in the iron parts of the machine.

By performing a simulation on the same machine with three phase currents (by running the *Reactances Study*-preset), the Synchronous Inductance is found by the Energy Method to be

$$L = 6.723\,\mathrm{mH}.$$

The same value is also obtained by subtracting the two former inductances, which is in accordance with Equation 34.

2) Distributed Winding: The number of slots is increased to 180 (30 slots per pole) to arrive at a distributed winding with a smooth air gap flux, expected to be similar to a trapezoidal wave. The inductances resulting from Equation 37 should provide a reasonable approximation in this case, as a trapezoidal wave to some extent resembles a sinusoidal wave.

All the added coils are connected in parallel, causing the total number of series connected turns in the machine to be the same, thus keeping the inductances at about the same level as those in the previous machine.

The Single Phase- and Three Phase Magnetizing Inductances are found analytically by Equation 37 and Equation 38,

$$L_{m,1ph} = 3.466\,\mathrm{mH},$$
$$L_{m,3ph} = 5.199\,\mathrm{mH},$$

Performing a similar single phase excitation procedure as for the previous case gives the Self- and Mutual Inductances

$$L_s = 3.524\,\mathrm{mH}$$
$$M = -1.490\,\mathrm{mH},$$

and using the Energy Method to calculate the Synchronous Inductance gives

$$L = 5.01\,\mathrm{mH}.$$

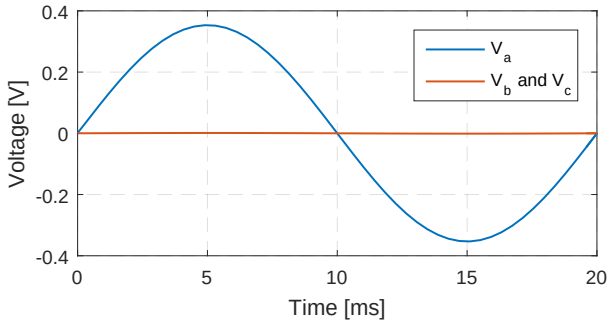

Figure 9: Voltage Induction during Single Phase Excitation in 10p, 12S machine with a Single Layer Fractional Slot Concentrated Winding. Only phase A is excited with a current of 1 A.

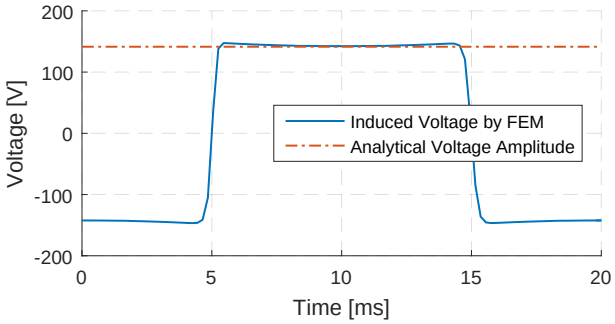

Figure 10: No Load Induced Voltage in 2p, 6S machine with a Single Layer Concentrated Winding.

The analytical value for Three Phase Magnetizing Inductance is higher than the Synchronous Inductance resulting from FEM, which is opposite of what is expected. However, the values are well in range, with the discrepancy possibly caused by non-zero reluctance of iron.

Self Inductance decreases from the case with the concentrated winding, which is expected due to the reduced magnitude of the air gap flux resulting when distributing the turns over multiple slots, rather than concentrating them in two slots.

The Mutual Inductance is about the same size as the previous case, but the Single Phase Magnetizing Inductance appears to have decreased. This makes sense when comparing the winding to a sinusoidally distributed winding: Mohan [12] shows that with a sinusoidal distribution, the Single Phase Magnetizing Inductance is twice the Mutual Inductance, rather than the triple, which is the case for full pitch concentrated windings (Equation 36). Due to a distributed winding more closely resembling a sinusoidally distributed winding than a concentrated winding, this result is not unexpected.

Finally, the relation described by Equation 34 holds also in this case, in that the difference of Self- and Mutual Inductances equals the Synchronous Inductance.

3) Fractional Slot Concentrated Winding: An analytical comparison concerning inductances for fractional slot concentrated windings is not performed here. However, a short inductance assessment is performed for a 10p, 12S machine, emphasizing that the relation between Self-, Mutual- and Synchronous Inductances still holds.

The number of poles and slots of the same machine are modified according to this, and the same procedure as above is carried out:

Single phase excitation yields the voltages in Figure 9. As expected, the mutual coupling between phases is essentially zero due to non-overlapping coils. Inductances are found to be

$$L_s = 1.124\,\mathrm{mH}$$

$$M = 0.0035\,\mathrm{mH}.$$

The Energy Method during three phase excitation gives

$$L = 1.121\,\mathrm{mH},$$

which indicates that the relation described by Equation 34 is valid also for fractional slot concentrated windings. The Synchronous Inductance is lower than the Self Inductance due to a positive Mutual Inductance, meaning that the flux contribution from the two other phases during three phase operation is negative.

B. Induced Voltage in Ideal Doubly Cylindrical Machine

The machine is again set to have 2 poles and 6 slots. The internal generated voltage is found by running a *No Load, Electrical Period*-preset, with the PMs activated. The analytical approximation is found by using Equation 29,

$$E = 149.3\,\mathrm{V}. \tag{42}$$

Plotting the induced voltage, shown in Figure 10, indicates good correlation between analytical calculations and FEM results. The amplitude of the voltage from FEM is about 144 V, which is slightly lower but well in range of the analytical value.

Further, the setup is augmented a series of times to see how the induced voltage changes along with the analytical approximation, presented in the table below.

Table III: Induced Voltage Comparison

	Analytical	FEM
Initial Setup	149.3	144
Doubling poles and slots	74.61	73.5
Doubling air gap length	47.12	47.8
Inserting 3 additional coils	188.5	191

The correlation is quite good. When doubling the number of poles the velocity of the rotor is halved, resulting in half the induced voltage (there is still only one coil). Doubling the air gap length (by reducing the size of the rotor) results in a value of about $\frac{2}{3}$ of the previous value, due to the increased air gap reluctance. Finally, inserting 3 additional coils, placed at electrically equivalent angles, and connecting them in series results in a quadrupled voltage.

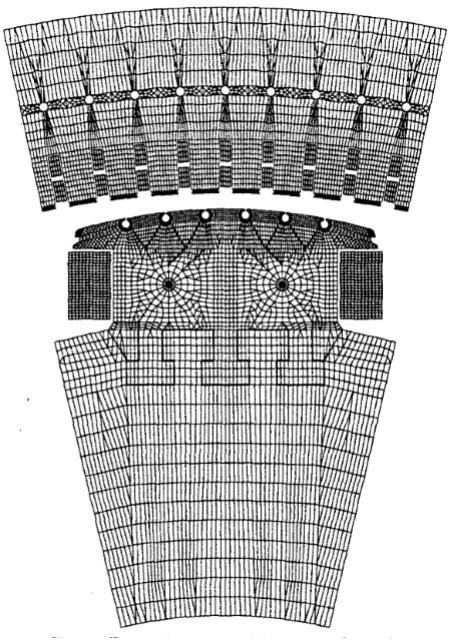

Figure 11: Schematic showing geometry of Bieudron Generators. Source: [16]

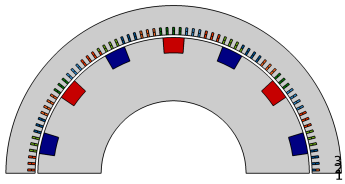

L	2900 mm
$R_{s,out}$	3240 mm
$R_{s,in}$	2675 mm
$R_{r,out}$	2622 mm
$R_{r,in}$	1400 mm
p	14
Q	138
S_d	145 mm
S_w	0.3125
R_{PM}	2325 mm
PM_h	297 mm
PM_w	0.35
PM_{br}	1.2 T
$N_{t,coil}$	1
N_{par}	2

Figure 12: Model of Bieudron Generator

C. Recreating a study on the Bieudron Generators

There is a lot of information available on the generators of the Bieudron Hydro Power Plant in Switzerland [15]. In addition, studies on the reactances of these are available [16]. Even though the construction differs slightly from what can be achieved with this model, a study is performed attempting to calculate the reactances of the generator.

It should be noted that the rotor field in these generators is set up by field windings instead of PMs; the machine is in this respect out of the scope of this model. However, due to the inductances being independent of field excitation (when saturation is not taken into account), they can be calculated regardless of this.

The machine has salient poles. To achieve this with the limited geometry variations of this model, the PMs are placed where the rotor slots in the original machine are situated. The flux remanence is deactivated, making the area that the PMs occupy behave similar to air (due to relative permeability equal to one, subsection III-C), resulting in a geometry resembling salient poles. The complete geometry is constructed based on the schematic shown in Figure 11, resulting in the model in Figure 12.

To calculate the d- and q-axis reactances, the *Reactances Study, d- and q-axis*-preset is loaded; the flux remanence of the PMs is set to zero, and a parametric study is initiated with two different values of u, corresponding to current in the d-axis and q-axis respectively. The resulting field distributions shown in Figure 13 clearly indicates a higher d-axis reactance. The values are found using the Energy Method (plotted in the Application by selecting Reactances in Evaluation) and presented in Table IV, along with values from the study by Schmidt et al. The correlation appears to be quite good, the minor error probably caused by small geometry differences.

Table IV: Bieudron Generator Reactances

	Result	Study by Schmidt et al.	Error
X_d	1.084 Ω	1.122 Ω	3.38%
X_q	0.725 Ω	0.795 Ω	8.81%

D. Smart Motor Machine with Concentrated Windings

Table V shows the relative errors from a study attempting to recreate the performance specific machine being developed by Smart Motor in Trondheim, Norway. Due to confidentiality reasons, no concrete input parameters or results are reproduced here; rather only the relative errors are shown, giving an impression of the accuracy of the model.

Table V: Study Replication on Smart Motor Machine

Parameter	Relative Error
V	-0.49%
τ	6.74%
P	6.74%
PF	0.37%
E	6.02%
X	-6.69%

PF is power factor. The model appears to be well capable of approximating the performance of this machine. However, some discrepancies appear, presumably due to the geometry of the original machine being somewhat more complex in some areas.

VI. Sample Studies

The discussion in the previous section indicates that the Application is able to produce valid results. This section presents a range of studies conducted with the purpose of indicating how the application could be used for studying

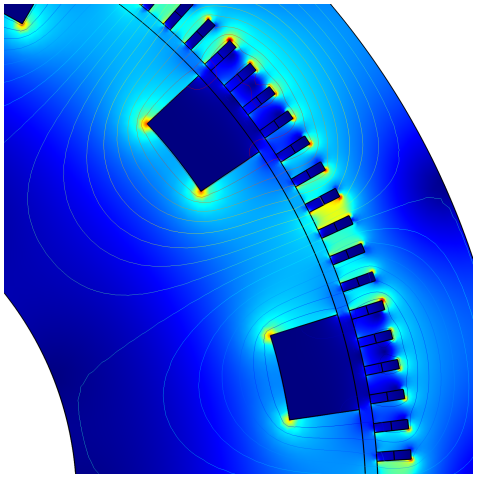

(a) d-axis current

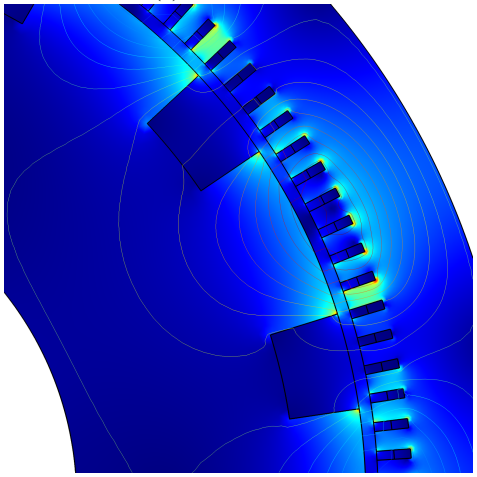

(b) q-axis current

Figure 13: Magnetic Flux Density in Bieudron Generator; 14p, 138S Double Layer Fractional Slot machine with Salient Poles. d-axis reactance is larger than q-axis reactance.

different machine phenomena. This also serves to further validate the output of the Application, as any inconsistency in the results would quickly be revealed.

A. *Machine with Inset PMs in rotor*

A study is conducted to assess the performance of a machine with Inset PMs [5] in the rotor, shown in Figure 14. The motivation for such a configuration could in practice be to enhance the ability of the rotor to withstand the centrifugal forces associated with high speed applications. The purpose of presenting the study here is merely to show the effect of unequal reactances along the d- and q-axis. Running a *Reactances Study, d- and q-axis*-preset study on this geometry yields the flux distributions shown in Figure 15, which clearly indicates a lower d-axis reactance. The reactance values are found by the Energy Method, which gives the values

$$X_d = 8.38\,\Omega$$
$$X_q = 16.02\,\Omega$$

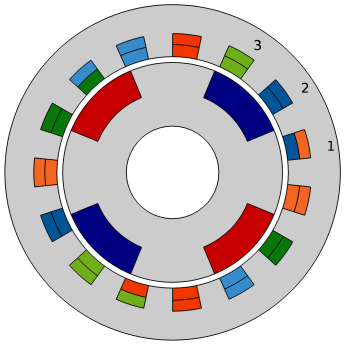

L	100 mm
$R_{s,out}$	145 mm
$R_{s,in}$	100 mm
$R_{r,out}$	95 mm
$R_{r,in}$	40 mm
p	4
Q	15
S_d	20 mm
S_w	0.5
R_{PM}	70 mm
PM_h	25 mm
PM_w	0.5
PM_{br}	1.2 T
$N_{t,coil}$	50
N_{par}	1

Figure 14: Model of machine with Inset PMs

Running the *Reactance Study, Continuous Variation*-preset, the current angle is varied continuously between the d- and q-axis, allowing the continuous reactance variation to be plotted, shown in Figure 16. The reactances can also be calculated by running the *Parameter Estimation*-preset, performing two simulations in time, respectively load and no load, and calculating the reactances from the equivalent circuit. This is accessible from the Phasor Diagram pane, resulting in the values

$$E = 380.62\,\text{V}$$
$$X_d = 8.22\,\Omega$$
$$X_d = 15.83\,\Omega,$$

which corresponds well with the values produced by the Energy Method.

The reactance being lower in the d-axis than the q-axis results in a negative contribution to the total torque, which is opposite of what is achieved with salient poles. This is further investigated by running a *Load, Torque Characteristic (fast)* preset study. Since this is a fractional slot-machine, the torque ripple is assumed to be negligible, yielding stationary studies sufficiently accurate. The preset initiates a parametric study which varies the angle of the current around the no load point, similarly to the preset performed above, but with the PM flux remanence reintroduced.

From Equation 20 it can be observed that if the internal generated voltage E is zero, the torque is constituted solely by the reluctance torque. This indicates that by performing a similar *Torque Characteristic* study with the PM flux remanence set to zero, the reluctance torque can be obtained directly.

Plotting the torque as a function of the current angle relative to the d-axis for the two cases, with and without flux remanence, gives the characteristics shown in Figure 17. In addition, the cylindrical torque is calculated by subtracting the reluctance torque from the full torque. The same characteristics can also be plotted by inserting the parameter values calculated

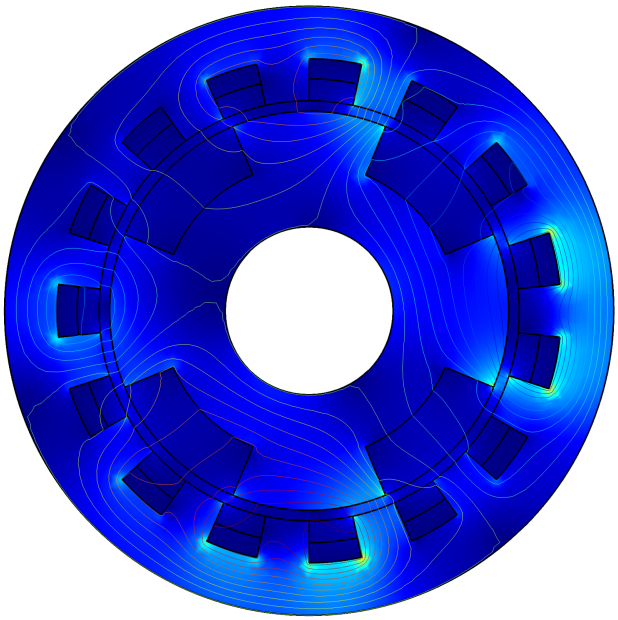

(a) d-axis current

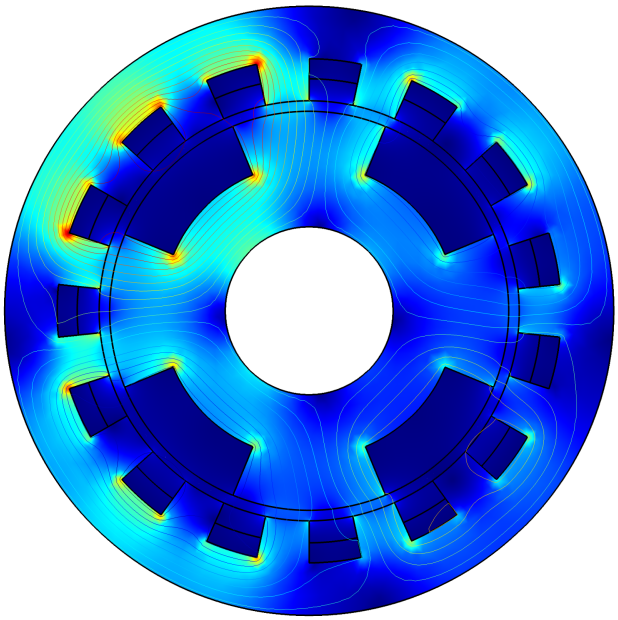

(b) q-axis current

Figure 15: Magnetic Flux Density machine with Inset PMs; 4p, 15S, Double Layer Fractional Slot Winding. q-axis reactance is larger than d-axis reactance.

above into Equation 20, which is shown with dashed lines in Figure 17.

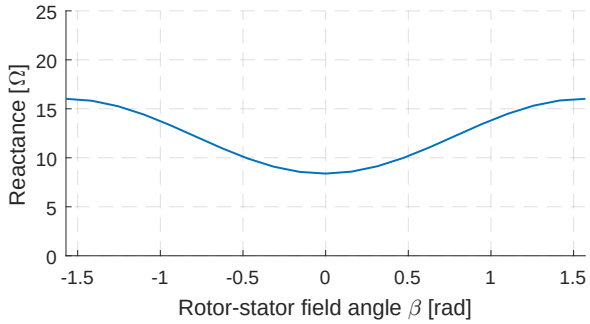

Figure 16: Reactance variation for different current angles relative to rotor field in PM machine with Inset PMs in rotor. $\beta = 0$ corresponds to d-axis current, $\beta = \pm\frac{pi}{2}$ to q-axis current.

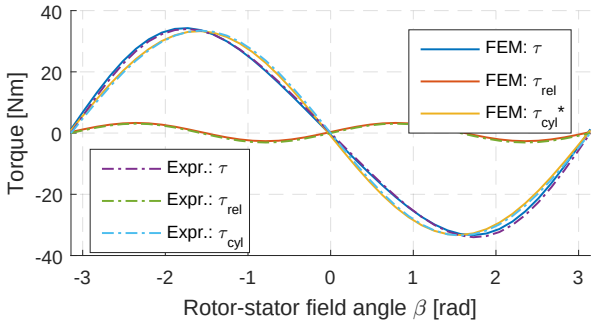

Figure 17: Torque Characteristic of PM machine with Inset PMs in rotor, displaying full torque, reluctance torque and cyllindrical torque.

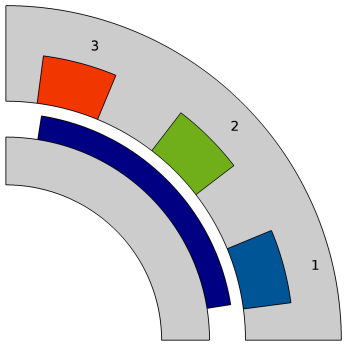

L	100 mm
$R_{s,out}$	140 mm
$R_{s,in}$	100 mm
$R_{r,out}$	85 mm
$R_{r,in}$	65 mm
p	4
Q	12
S_d	20 mm
S_w	0.5
R_{PM}	85 mm
PM_h	10 mm
PM_w	0.4-1
PM_{br}	1 T
$N_{t,coil}$	100
N_{par}	1

Figure 18: Model for PM Width Study

B. PM Width Influence on No Load Cogging Torque and Induced Voltage

A study is performed to assess how PM width influences cogging torque and no load induced voltage waveforms in a 4p, 12S-machine, shown in Figure 18. Considering cogging

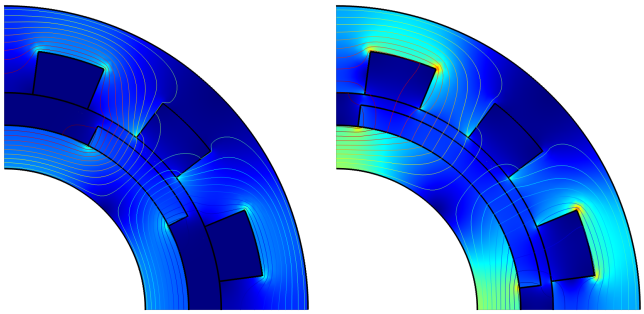

(a) Relative PM width = 0.4 (b) Relative PM width = 0.8

Figure 19: Magnetic Flux Density for two different PM widths in a 4p, 12S, Single Layer Integer Slot machine.

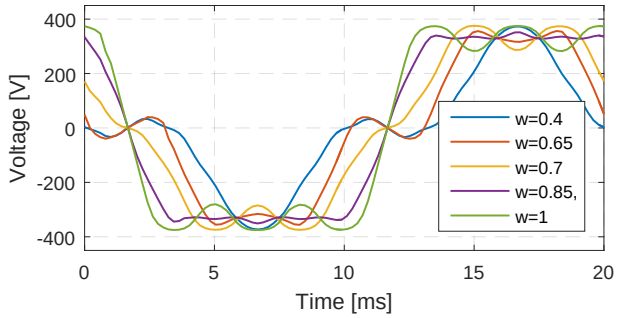

Figure 20: PM Width influence on No Load Induced Voltage.

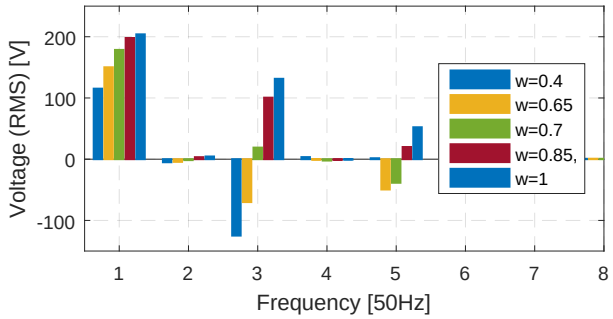

Figure 21: PM Width influence on harmonics in No Load Induced Voltage, simulated over one electrical period.

torque, the *No Load, Cogging Torque Cycle*-preset is loaded, which sets the simulation time according to Equation 16, such that only one cycle is simulated. Considering no load induced voltage, one complete electrical cycle is simulated (study preset *No Load, Electrical Period*). In addition, the parametric sweep option is activated, with five different values ranging from 0.4 to 1 being assigned to the parameter u. Finally, the PM width is set equal to u.

Figure 19 shows the magnetic flux density in two of the resulting cases, for relative PM widths of 0.4 and 0.8. The larger PMs cause a higher flux density in the rotor and stator yokes. This also produces a higher fundamental component

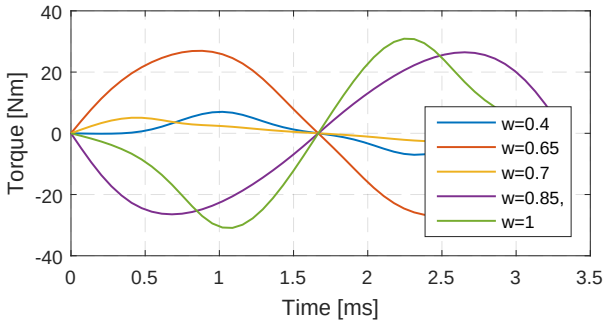

Figure 22: PM Width influence on Cogging Torque, simulated over one cogging torque cycle.

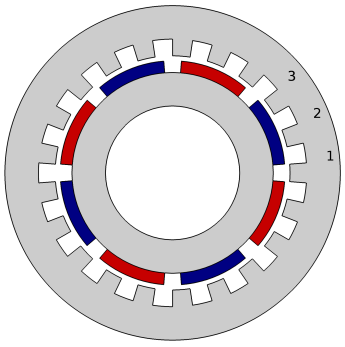

L	100 mm
$R_{s,out}$	500 mm
$R_{s,in}$	350 mm
$R_{r,out}$	300 mm
$R_{r,in}$	200 mm
p	8
Q	9-21
S_d	50 mm
S_w	0.5
R_{PM}	300 mm
PM_h	35 mm
PM_w	0.8
PM_{br}	1 T

Figure 23: Model for Cogging Torque Study, varying Q

of the voltage, which is shown in Figure 20, and in the Fourier decomposition of the voltage, in Figure 21. The latter also indicates that the third harmonic is significantly affected by PM width, which is quite intuitive: Whereas a negative third harmonic, associated with the lower PM widths, would contribute positively to the extremes of the fundamental and negatively to the slopes, a positive third harmonic would do the opposite, approaching a square wave.

Regarding cogging torque, it appears that significant improvements can be achieved by optimizing the width of the PMs. Figure 22 shows the cogging torque wave forms resulting from this study, where the relative widths of 0.4 and 0.7 clearly stand out as better choices for minimizing torque ripple. The period of one cycle is 3.33 ms, which is in accordance with Equation 16.

Thus, for this particular setup, it appears that a relative PM width of 0.7 is the best choice among the five alternatives, both for minimizing cogging torque and harmonics content. The study could be taken further, performing the same routine with widths centered more closely around 0.7, providing a more optimal value.

C. Poles-Slots Combination influence on Cogging Torque

A study is conducted to assess the cogging torque in a 8 pole machine with different numbers of slots. The model is

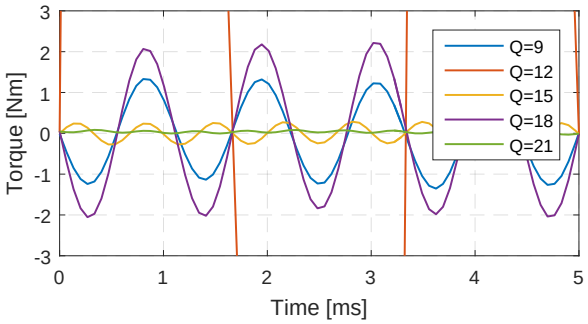

Figure 24: Cogging Torque for different numbers of stator slots in machine with 8 poles.

shown in Figure 23 for a variant with 21 slots. A parametric, time dependent study is initialized, where the number of slots is set equal to u, which is assigned the values 9, 12, 15, 18 and 21. These are all combinations for which a double layer symmetric three phase winding layout can be performed. However, the winding is deactivated for this case, as the focus of the study is cogging torque. Also, the winding layout would not update between iterations in a parametric study (mentioned in subsection IV-B).

The study results in torque wave forms shown in Figure 24. The differences are quite large, with the 12 slot-variant resulting in a torque ripple with amplitude 101 Nm, which is about 45 times larger than the next largest ripple (which is why it is not shown entirely in the figure). The 21 slot-variant has the smallest ripple. The results are summarized in Table VI, along with theoretical values describing torque ripple, presented in subsection II-F.

Table VI: Cogging Torque Study Results

Q	$\mathtt{lcm}(Q,p)$	Period [ms]	Amplitude [Nm]
9	72	1.1	1.38
12	24	3.3	101
15	120	0.7	0.284
18	72	1.1	2.21
21	168	0.5	< 0.01

It is found that the amplitude in general decreases with $\mathtt{lcm}(Q,p)$, which is also indicated by Hwang et al. [9]. The ripple cycle period is calculated using Equation 16, and agrees well with the results. The amplitude of the 21 slot-variant is smaller than $0.01\,\mathrm{Nm}$, but appears to contain a fluctuating DC-component (or some sub harmonic frequency).

The study thus indicates how introducing a fractional slot configuration can be used as a means of minimizing cogging torque.

D. Mesh Density influence on Cogging Torque Accuracy

A study is conducted to assess the no load cogging torque in a 14p, 15S machine, emphasizing the influence that the element density of the mesh has on the accuracy of the result. Also, a comparison of using Maxwell Stress Tensor and Arkkios Method is performed. The model is shown in Figure 25.

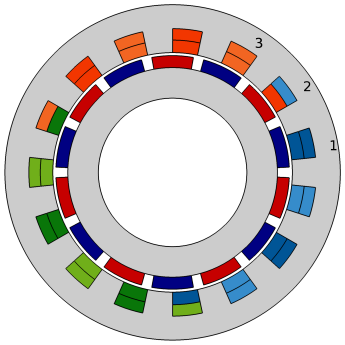

L	100 mm
$R_{s,out}$	140 mm
$R_{s,in}$	100 mm
$R_{r,out}$	87.5 mm
$R_{r,in}$	62 mm
p	14
Q	15
S_d	20 mm
S_w	0.5
R_{PM}	87.5 mm
PM_h	10 mm
PM_w	0.8
PM_{br}	1.2 T
$N_{t,coil}$	100
N_{par}	1

Figure 25: Model for Mesh Density Study

This particular poles/slots-combination results in a machine with no periodicity, requiring the complete geometry to be modeled. Also, the amplitude of the torque ripple is expected to be low, due to the high value of $\mathtt{lcm}(Q,p) = 14 \cdot 15 = 210$. This requires the element density along the air gap to be high to keep distortion along the stator/rotor boundary to a level where it does not influence the torque ripple.

The study is initiated by loading the *No Load, Cogging Torque Cycle*-preset, setting the simulating time to one cogging torque cycle. In addition, a parametric study is set to increase the element density in the air gap gradually over five simulations by setting the number of boundary layers equal to u. The resulting torque wave forms are shown for different meshes in Figure 26a and Figure 26b, calculated by using Maxwell Stress Tensor and Arkkio's Method respectively. The density of the mesh is indicated by the number of degrees of freedom of the FEM-problem (dofs), which is roughly three times the number of elements of the mesh (three vector potential components for each element).

It appears that both methods arrive at the same result for the denser meshes. Using Maxwell Stress Tensor gives a large error for the coarser meshes, but provides a smooth result. Arkkio's Method produces a smaller overall error, but contains a significant amount of noise for the coarser meshes. Figure 27 shows how the error decreases with an increasing amount of elements. The error is calculated from the difference between the respective signals and the most accurate solution. The total error is expressed as the L^2-norm [19] of the error as a function of time, given by the following equation,

$$|e| = \sqrt{\sum_{i=0}^{N} e_i^2} = \sqrt{\sum_{i=0}^{N} (x_i - x_i^*)^2}. \tag{43}$$

In this case, x_i denotes the torque of the solution being

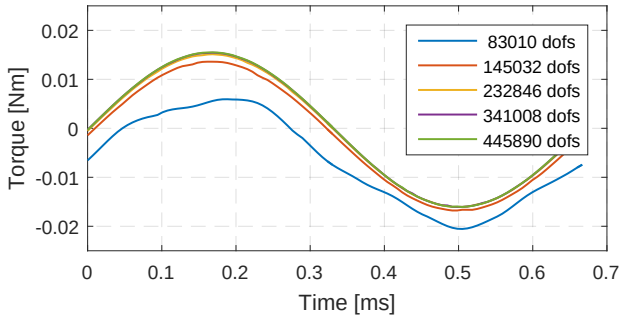

(a) Maxwell Stress Tensor

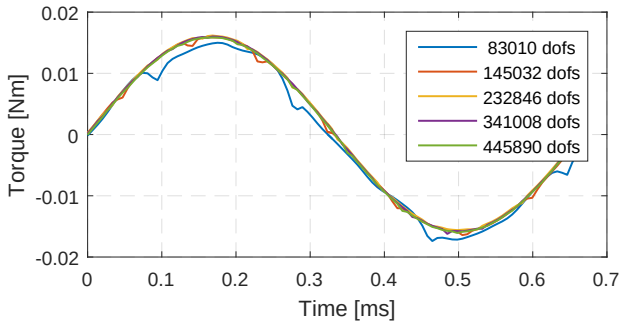

(b) Arkkio's Method

Figure 26: 14p, 15S machine, Cogging Torque wave form for various element densities, corresponding to Number of Degrees of Freedom (dofs)

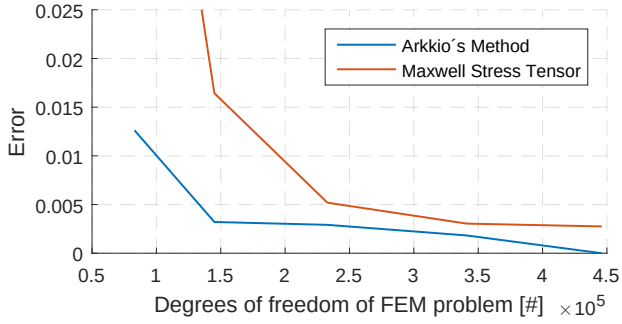

Figure 27: 14p, 15S machine, Cogging Torque Error plotted as function of Degrees of Freedom of FEM problem.

investigated, and x_i^* denotes the torque of the most accurate solution. Index i denotes evaluation at time instant t_i, and N is the number of stored time instants. The most accurate solution is chosen to be the one calculated by Arkkio's Method at the highest element density, due to the DC-component of the signal, which should be zero under no load, being slightly lower than for the result computed using Maxwell Stress Tensor.

The noise appearing in the results calculated by Arkkio's Method is likely caused by the element density along the stator/rotor boundary being too low. Plotting the magnetic flux density along this boundary reveals that the field is highly distorted, and as the torque is calculated by integrating over the region containing this boundary, it is highly prone to this noise. This indicates that the division of regions in the air gap is not optimal for this type of calculations. If the integration region instead was placed such that it did not contain the stator/rotor boundary, it would most likely produce a smoother output.

VII. Discussion

The studies presented in the previous sections demonstrate how the Application could be used in an educational setting. It is found that simulations can be performed very efficiently due to automatic winding layout, symmetry settings, construction of geometry and result handling. When working without this functionality, a significant amount of time is spent on the process of specifying input manually; finding a winding layout, entering the six phase polarity-vectors, activating and deactivating the required symmetry settings, and so on.

The option of performing geometric parametric sweeps allows the same simulation, time dependent or stationary, to be performed for a range of slightly different machines. The time instants and sweep variable values corresponding to the resulting sub-solutions can then be browsed through very easily. When viewing results in tiled view, i.e. viewing results side by side, the surface plots of magnetic flux density can be viewed alongside, for instance, induced voltage. This serves very well to give an intuitive understanding of how geometrical choices affect performance of a machine, for instance regarding harmonics in the induced voltage for different PM widths, as discussed above. In an educational setting this could be utilized in a number of ways; relating torque production to machine size by scaling the whole machine between iterations, relating reactance variation to air gap length, internal generated voltage to rotational speed, and so on.

The same functionality could also be used by a machine designer, allowing optimization decisions to be made very quickly. An Optimization Module is also available in COMSOL, which could be interesting to combine with the parametrized model developed.

There is still a large potential for improvements, and for functionality to be added to the model. At this point the setup is relatively simple in many ways, in that a lot of significant phenomena are neglected; resistive losses and saturation could easily be incorporated into the model, merely requiring the activation of a setting. More fundamental changes could also be made, for instance to take mechanical dynamics into account; this could be done by assigning a finite inertia to the rotor, and specifying the input as a load torque rather than rotor angle.

The geometrical choices available are also quite limited. The next step that should be taken with respect to this is probably to allow field windings and salient poles. It should be noted that as the geometrical choices increase, so does the complexity of the model, which requires an increasing amount of attention to be paid to ensuring that the model builds properly, and that the right selections are defined.

Regarding the implemented GUI of the Application, some parts are more successful than others. The panes for Geometry and Simulation input are relatively well functioning. Regarding the Results pane, the way that the phasor diagram functions (requiring the user to manually input reactances and internal generated voltage, or to run a specific study and calculate them), is perhaps not the most elegant. Another way this could be done would be to set up a more sophisticated solver sequence that calculated the reactances automatically (from the Energy Method) before each time dependent or stationary study, as this is done in a matter of seconds anyway, and then automatically used these in the phasor diagram.

The testing that the Application has gone through so far is limited, such that it is expected to contain bugs and errors. One obvious flaw that should be fixed is that when performing a parametric sweep where a geometry variable is defined as a function of the sweep variable u, then the routine that checks whether the geometry parameters are valid is run only for the first value of the sweep variable. Incompatible geometry parameters could result in the geometry sequence being corrupted, which would require it to be fixed from within the Model.

VIII. Conclusion

It appears that the Application could provide a valuable tool, first and foremost in an educational setting, but if developed further probably also by engineers in the process of designing machines. First, and most important, results provided by the model appear to be consistent, and to correlate well with both analytical formulas and with other similar studies. Second, simulations can be performed very efficiently with the automated functionality implemented. Especially due to the ability of performing geometric parameter sweeps, the Application could serve to relate geometrical choices to machine performance, and to allow optimization decisions to be made.

Due to a lack of extensive testing, the Application is expected to contain bugs and errors. It should in this respect be considered a work in progress. Apart from this the performance is promising, which motivates further development to expand geometry variation possibilities, and to incorporate functionality for calculating losses.

References

[1] Antero Arkkio. *Analysis of Induction Motors Based on the Numerical Solution of the Magnetic Field and Circuit Equations*. PhD thesis, Helsinki University of Technology, 1987.

[2] R. Bargallo, J. Llaverias, A. De Blas, H. Martn, and R. Piqué. Main inductance determination in rotating machines. analytical and numerical calculation: A didactical approach.

[3] N. Bianchi and M. Dai Prè. Use of the star of slots in designing fractional-slot single-layer synchronous motors. *IEE Proceedings - Electric Power Applications, Vol. 153, No. 3*, 2006.

[4] Stephen J. Chapman. *Electric Machinery Fundamentals, Fifth Edition*. McGraw-Hill, 2012.

[5] Jacek F. Gieras. *Permanent Magnet Motor Technology*. CRC Press, Taylor & Francis Group, 2010.

[6] B. L. J. Gysen, K. J. Meessen, J. J. H. Paulides, and E. A. Lomonova. General formulation of the electromagnetic field distribution in machines and devices using fourier analysis. *IEEE Transactions on Magnetics, Vol. 46, No. 1*, 2010.

[7] Duane C. Hanselman. *Brushless Permanent-Magnet Motor Design*. McGraw-Hill, 1994.

[8] Chun-Yu Hsiao, Sheng-Nian Yeh, and Jonq-Chin Hwang. A novel cogging torque simulation method for permanent-magnet synchronous machine. *Energies, Vol. 153*, 2011.

[9] C.C. Hwang, M.H. Wu, and S.P. Cheng. Influence of pole and slot combinations on cogging torque in fractional slot pm motors. *Journal of Magnetism and Magnetic Materials*, (304), March 2006.

[10] Thomas A. Lipo. *Analysis of Synchronous Machines*. Wisconsin Power Electronics Research Center, University of Wisconsin, 2008.

[11] Jan Machowski, Janusz W. Bialek, and James R. Bumby. *Power System Dynamics*. John Wiley & Sons, Ltd, 2012.

[12] Ned Mohan. *Advanced Electric Drives*. MNPERE, 2001.

[13] Øystein Krøvel. *Design of Large Permanent Magnetized Synchronous Electric Machines*. PhD thesis, Norwegian University of Science and Technology, 2011.

[14] Juha Pyrhönen, Tapani Jokinen, and Valéria Hrabovcová. *Design of Rotating Electrical Machines*. John Wiley & Sons, Ltd, 2008.

[15] Daniel Schafer. The world's largest fully water cooled hydro generators in the Bieudron power plant (Switzerland). *International Conference Electric Machines and Drives*, 1999.

[16] Erich Schmidt, Christan Grabner, and Georg Traxler-Samek. Finite element analysis of the 500 mva hydrogenerators at the Bieudron power plant. *Proceedings of the Fifth International Conference on Electrical Machines and Systems, Vol. 2*, 2001.

[17] Heinrich Sequenz. *Die Wicklungen elektrischer Maschinen*, volume Erster Band. Springer-Verlag, 1950.

[18] P. P. Silvester and R. L. Ferrari. *Finite Elements For Electrical Engineers*. Cambridge University Press, 1990.

[19] John C. Strikwerda. *Finite Difference Schemes and Partial Differential Equations*. Wadsworth & Brooks/Cole Advanced Books & Software, 1989.